REVIEW

Check for updates

Regulation engineering of the surface and structure of perovskite-based electrocatalysts for the oxygen evolution reaction

Ning Yu, Zhi-Jie Zhang, Yong-Ming Chai* and Bin Dong (ID) *

Perovskite oxides of low cost and with an adjustable structure have been widely used as electrocatalysts for the oxygen evolution reaction (OER). However, most perovskite oxides have inherent barriers of low catalytic activity and poor electrical conductivity. The reaction at the active site and the adsorption/desorption of the reactants are carried out more efficiently on the catalyst surface. In order to regulate the surface and structure of a catalyst to improve the catalytic activity of perovskite oxides in the OER, many strategies have been explored. In this paper, the descriptor of catalytic activity of perovskite oxides is described. The oxygen evolution mechanisms (the adsorbate evolution mechanism, AEM, and lattice oxygen evolution mechanism, LOM) and the regulation mode between AEM and LOM have been deeply analyzed to guide the design of high performing catalysts for the OER. The research progress of perovskite oxide catalysts in recent years in terms of surface composition, design morphology control and defect engineering is reviewed systematically. In particular, the Ir/Ru perovskite in acidic media that can be used in a proton exchange membrane water electrolyser (PEMWE) is discussed in detail. Finally, the existing problems of perovskite oxide based electrocatalysts and their prospects for practical applications in the OER are presented.

1. Introduction

Clean and renewable energy technologies have been rapidly developed to address serious environmental problems caused by excessive consumption of non-renewable resources such as

State Key Laboratory of Heavy Oil Processing, College of Chemistry and Chemical Engineering, China University of Petroleum (East China), Qingdao 266580, P. R. China. E-mail: ymchai@upc.edu.cn, dongbin@upc.edu.cn; Fax: +86-532-86981156; Tel: +86-532-86981156

natural gas, oil and coal.[1,2] Hydrogen is an ideal renewable energy source with zero pollution. Electrochemical water decomposition hydrogen production ($H_2O \rightarrow H_2 + 1/2O_2$) is widely regarded as one of the most attractive sustainable energy conversion and storage technologies.[3–5] Essentially, the existence of slow multistep proton-coupled electron transfer in the oxygen evolution reaction (OER) prevents the realization of hydrogen production for efficient water electrolysis. Noble metal catalysts, such as RuO_2 and IrO_2, show excellent OER

Ning Yu received her BS degree from Liaocheng University. She is pursuing her PhD under the supervision of Professor Bin Dong in the State Key Laboratory of Heavy Oil Processing, College of Chemistry and Chemical Engineering, China University of Petroleum (East China). Her research interests focus on the perovskite-based nanomaterials for electrocatalysis for water electrolysis.

Ning Yu

Zhijie Zhang received her BS degree from Liaocheng University. She is pursuing her master's degree under the supervision of Professor Bin Dong in the State Key Laboratory of Heavy Oil Processing, College of Chemistry and Chemical Engineering, China University of Petroleum (East China). Her research interests focus on transition metal-based nanostructures for electrocatalysis for water splitting.
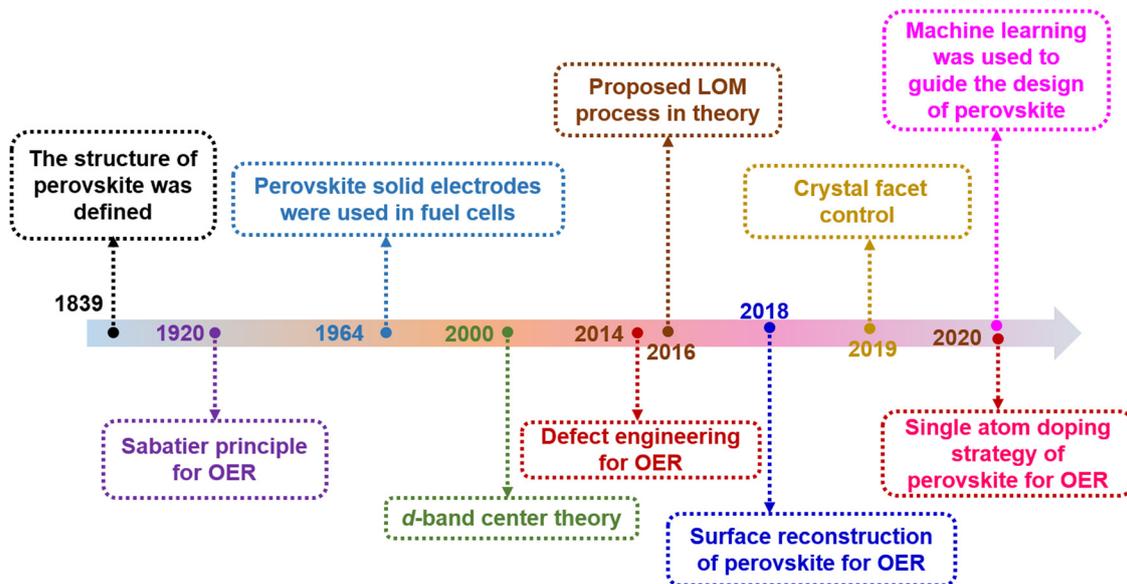
Zhi-Jie Zhang

This journal is © The Royal Society of Chemistry and the Chinese Chemical Society 2023

Fig. 1 The timeline-based accomplishments in the exploration of perovskite oxides for the OER. All the data were searched for in the Web of Science Core Collection.

performance, but their high cost in practical applications seriously hinders their widespread application.[6,7] This challenge has ignited a surge of research to find cost-effective and durable non-precious transition metal oxides as electrocatalysts for OERs.

In 1839, a mineral composed of calcium titanate ($CaTiO_3$) was first discovered from skarn by the Prussian mineralogist Gustav Rose, who named it after the mineralogist L. A. Perovski. To date, significant progress has been made in the in-depth understanding of the reaction mechanism of perovskite-based catalysts and in the design of efficient catalysts (Fig. 1). The typical single perovskite $Ba_{0.5}Sr_{0.5}Co_{0.8}Fe_{0.2}O_{3-\delta}$ (BSCF) exhibits higher intrinsic activity in alkaline electrolytes than the

Prof. Yong-Ming Chai received his PhD from China University of Petroleum (East China) in 2008. Now he is a professor and the deputy director of State Key Laboratory of Heavy Oil Processing, College of Chemistry and Chemical Engineering, China University of Petroleum (East China). He carried out research as a visiting scholar in Marquette University from 2015.03 to 2016.03. His research interests focus on transition metal-based

Yong-Ming Chai

catalysts for the utilization and production of green hydrogen including the hydrodesulfurization process of heavy oil and water splitting. Prof. Chai is an associate editor of Nano-Micro Letters, a Young Editorial Board Member of Journal of Fuel Chemistry and Technology.

Prof. Bin Dong received his BS and PhD from Lanzhou University in 2002 and 2008, respectively. He carried out research as a visiting scholar in Marquette University from March 2014 to March 2015. Now he is a Professor at the State Key Laboratory of Heavy Oil Processing, College of Chemistry and Chemical Engineering, China University of Petroleum (East China). His research interests mainly focus on transition

Bin Dong

metal-based functional materials for energy conversion and storage including electrocatalysis and photoelectrocatalysis. Prof. Dong has published more than 150 SCI papers including 7 ESI papers as the first-author or corresponding author with an H index 56. He was selected as a Highly Cited Chinese Researcher from Elsevier in 2022. Prof. Dong is an Editorial Board Member of Chinese Chemical Letters, an assistant editor of Nano-Micro Letters, a Young Editorial Board Member of Nano-Micro Letters, eScience, a Young Editorial Board Member of Chinese Journal of Structural Chemistry, and a member of the International Society of Electrochemisty.

IrO$_2$ reference in some cases.[8] A series of compelling dual perovskites with outstanding OER activity have been predicted and further evaluated by developing activity descriptor data-driven machine learning methods that can accelerate the design of highly active and low-cost electrocatalysts.[9] Perovskite oxides usually represent a class of materials with the general formula ABO$_3$ (A = alkaline, alkaline earth or rare earth metal, B = transition metal, and O = oxygen). Recently, perovskite oxides with ABO$_3$ rich in earth elements have attracted great interest in OER catalysis due to their high intrinsic activity and large composition/structure adjustability.[10–12] In the basic perovskite oxide structure, the B-site cations coordinate with the oxygen atom octahedron (BO$_6$), whose shared angles in the three directions of the crystal are located in the center of the cube (Fig. 2a). The A-site cations exhibit 12-fold coordination in the octahedral interspace. The perovskite crystal structure shows incomparable flexibility, which can incorporate almost all metal ions in the periodic table (about 90% of the elements in the periodic table) into the perovskite structure (Fig. 2b). Many studies have developed catalysts with double perovskites (A$_2$B$_2$O$_6$),[13] triple perovskites (A$_3$B$_3$O$_9$),[14] quadruple perovskites (A$_4$B$_4$O$_{12}$),[15] and Ruddlesden–Popper perovskites (A$_{n+1}$B$_n$O$_{3n+1}$ (n = 1, 2, and 3)).[16] The special structure and properties of perovskite offer several advantages in the OER: (1) Perovskite oxides have a robust crystalline structure that is highly stable under harsh reaction conditions, such as high temperatures and corrosive environments, making them suitable for use in the OER. (2) The electronic properties of perovskite oxides can be tuned by varying the composition of the A and B-site cations, allowing for the optimization of the electronic structure for OER catalysis. (3) The unique combination of metal cations in the perovskite structure can lead to synergistic effects that enhance the catalytic activity of the material, leading to improved OER performance. (4) Perovskite oxides can achieve high catalytic activity for the OER at low overpotentials, which is the extra energy needed to drive the reaction forward.

The special structure allows perovskite to exhibit properties comparable to those of Ir/Ru base standards.[17] Noble-metal base perovskite oxides in polymer electrolyte membrane (PEM) water electrolyzers have the advantages of a more stable structure and a lower noble metal content when running at a higher current density.[12,18] However, pure perovskite oxides (for example, LaNiO$_3$, LaCoO$_3$, LaFeO$_3$, etc.) as OER catalysts still have the disadvantages of poor conductivity and few active sites limiting their development in this field. Reducing the overpotential of the OER, or the energy level of the catalyst should be closer to the equilibrium potential of 1.23 V ($2H_2O(l) \rightarrow O_2(g) + 4H^+(aq) + 4e^-$, E^0 = 1.23 V), is frequently one of the criteria for measuring the catalytic activity in the design of catalysts.[19,20] The reaction can be initiated thermodynamically because the electron exchange between the electrocatalyst and the reactants is more favorable. Many effective strategies, such as hybridization, crystal facet control, morphology control, and defect engineering, have been applied to improve the intrinsic activity and stability of perovskite oxides for the OER. Perovskite oxides are widely used in catalysis, electrocatalysis and photocatalysis. They are also employed as components of devices that facilitate new energy innovations, such as catalytic metal–air cells,[21] water splitting,[22] and solid oxide fuel cells.[23]

Herein, the descriptor of catalytic activity of perovskite oxides is introduced. The recent strategy for adjusting the physical and chemical characteristics of perovskite oxides is described for application in OER. The catalytic mechanisms of the OER, including AEM and LOM, are deeply understood, and the regulation of the oxygen evolution mechanism is summarized. Strategies for improving the catalytic activity and stability of OER perovskite oxides are systematically studied, including composition engineering, morphology modulation, defect engineering, etc. In particular, the development of Ir/Ru-based perovskite oxide catalysts for PEMWEs under acidic environments is discussed. Finally, the challenges with employing perovskite oxides in practical applications as OER electrocatalysts are prospected.

2. Reaction mechanisms of perovskite-based electrocatalysts

2.1. AEM

The OER on the anode is one of the half reactions in the water cracking process, which is a 4-electron process. There are two widely accepted OER mechanisms, identified as the adsorbate
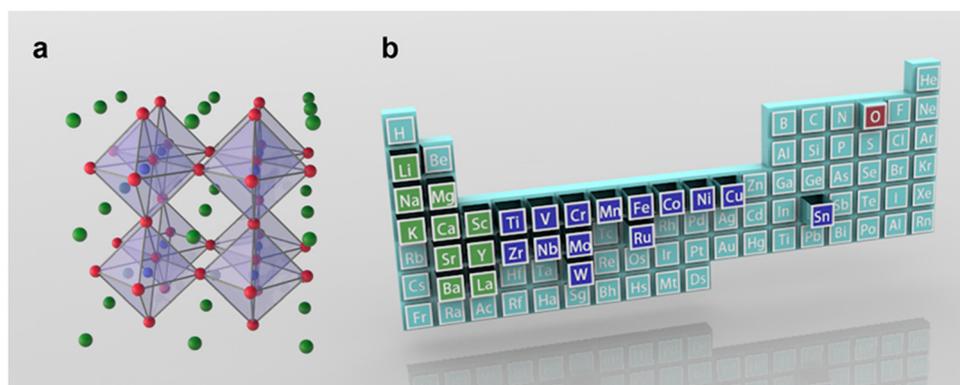

Fig. 2 (a) Schematic illustration of the structure for perovskites (ABO$_3$). (b) The commonly used element in perovskite oxides. Green is the A-site element, blue is the B-site element, and red is oxygen.

This journal is © The Royal Society of Chemistry and the Chinese Chemical Society 2023

evolution mechanism (AEM) and lattice oxygen evolution mechanism (LOM). OER behaves differently under acidic and alkaline conditions.

The AEM process occurs through multiple oxygen intermediates including OH*, O*, OOH*, and O_2, in which a series of consistent electron–proton transfer steps occur between the metal band and the adsorbent oxygen intermediate.[24–26] Because of this process, AEM is considered to be a metal redox catalytic reaction. For AEM, the OER is caused by water adsorption on the catalyst surface and subsequent hydrolytic dissociation. The important intermediates are M–O and M–OOH, which eventually produce oxygen.

Exploring the real active site in the catalytic process of OER catalysts is the focus of many researchers. In AEM, it is widely believed that the active site is a transition metal ion, at which water molecules are adsorbed and oxidation occurs (Fig. 3a). Many reports have shown that the presence of B-site metal ions in the octahedral structure of BO_6 in perovskite-type OER catalysts plays an important role in the catalytic process.[27,28] For example, Fe ions in perovskite oxides have been shown to be highly catalytic elements of the OER, and can be doped with Co to achieve higher catalytic performance.[28] According to Man *et al.*'s theoretical analysis, the activity of perovskite oxides presents volcanic maps in the following order: $SrCoO_3$ > $LaNiO_3$ > $SrNiO_3$ > $SrFeO_3$ > $LaCoO_3$ > $LaFeO_3$ > $LaMnO_3$.[29] This trend was also verified through experiments by Bockris *et al.* and Y. Matsumoto *et al.*[30,31] The perovskite oxide at the top of the volcano showed a better catalytic performance. Perovskite oxides on the left half of the volcano suggest a binding force that is too strong with the adsorbent, whereas perovskite oxides on the right half represent a binding force that is too weak. The best OER performance can only be attained at the active site with the appropriate adsorption intensity. In AEM, OER activity is independent of pH at the reversible hydrogen electrode (RHE) scale. Despite this progress, a number of issues remain to be resolved.

2.2. LOM

With the development of a large number of OER catalysts, it has been found that the OER catalytic activity of some materials does not follow the volcanic relationship. The active oxygen evolution activity of some catalysts depends on the pH in the electrolyte.[32,33] One explanation for the discrepancy is that these catalysts do not

actually follow the reaction mechanism described above. Inspired by this, the lattice oxygen oxidation mechanism (LOM) has been widely studied. Through theoretical calculation, Mefford *et al.* found that lattice oxygen was also involved in the OER process of $La_{1-x}Sr_xCoO_{3-\delta}$, which may explain the reason for its high activity. This mechanism has also been verified by experiments.[34] Shao-Horn *et al.* found that the oxygen produced in the OER process came from lattice oxygen on $SrCoO_{3-\delta}$, $Pr_{0.5}Ba_{0.5}CoO_{3-\delta}$ and $La_{0.5}Sr_{0.5}CoO_{3-\delta}$ by *in situ* ^{18}O isotope-labeled mass spectrometry.[32] In the LOM, the metal-lattice oxygen oxidation mechanism (M–LOM) and oxygen-lattice oxygen oxidation mechanism (O–LOM) are divided according to whether the active site is metal or lattice oxygen (Fig. 3b and c).[35] In the first step of M–LOM, –OO is formed by dehydrogenation at the transition metal site where –OH is adsorbed. On dehydrogenation, the O of the adsorbed –OH binds to the lattice O. In the third step of M–LOM, OO evolves into O_2, forming an oxygen vacancy. The oxygen vacancy is then filled by OH^-. Finally, deprotonation occurs and the initial surface is restored. There is decoupling of the proton–electron transfer step in the LOM due to oxygen vacancy generation, resulting in the pH-dependent OER properties previously observed. Shao-Horn *et al.* also proposed a new reaction mechanism (O–LOM, Fig. 3c), which is similar to M–LOM.[32] The main difference between M–LOM and O–LOM is that M–LOM assumes that the active site of perovskite is the metal site, whereas O–LOM assumes that it is the lattice-oxygen site.[36] Gao-Ren Li *et al.* established the relationship between lattice oxygen evolution reaction and dynamic surface structure.[37] Through theoretical calculations and *in situ* characterization, such as *in situ* X-ray absorption near edge structures (XANES) and *in situ* Raman, it has been demonstrated that surface Fe sites are catalytic centers of LOM, and Sr vacancies can promote the LOM by raising the 2p level of oxygen. To verify whether LOM is dominant in the OER: first, it is possible to test whether the catalyst performance is strongly dependent on pH; Secondly, the performance of catalysts with LOM is generally improved after the CV test. Third, direct isotope labeling is used to observe whether the O in the production of O_2 comes from lattice oxygen.

2.3. Regulation of the reaction mechanism

In LOM, O–O radical coupling is achieved directly without the involvement of M–OOH intermediates.[39] The process avoids the
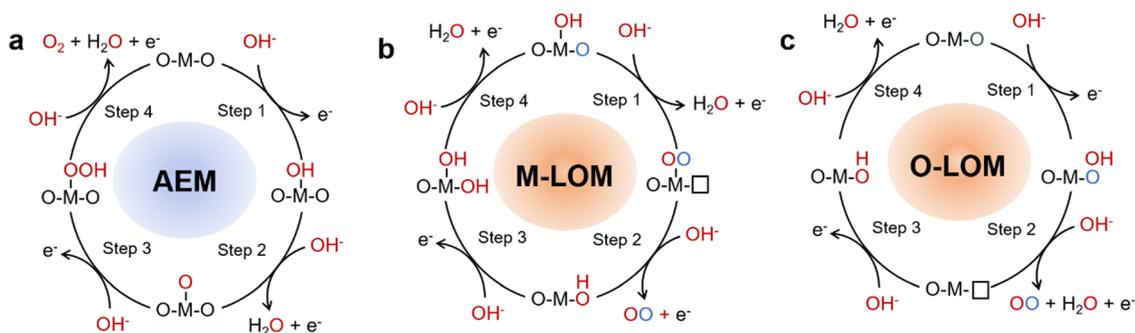

Fig. 3 Schematic OER mechanisms on perovskite oxides: (a) AEM, (b) M−LOM, and (c) O−LOM.

limitation of the adsorption energy scale, resulting in the catalyst working in LOM showing higher apparent activity than one working in AEM.[39–42] However, the catalyst is usually accompanied by a large amount of surface reconstruction during the LOM process due to the redox and overflow of lattice oxygen, which is very unfavorable to the stability of the catalyst.[38] Therefore, how to regulate the reaction path between AEM and LOM to achieve a coordinated symbiosis of catalyst activity and stability is a problem that needs to be considered for catalyst design.

The way InIch the OER mechaIism is regulated can be differentiated according to whether or not the chemical composition of the catalyst is changed. In general, people can optimize the reaction mechanism by changing the material of catalyst to regulate the distribution state of electrons or the adsorption energy of reaction intermediates. In the Mott–Hubbard cationic redox environment, when U (the energy difference between the empty upper Hubbard band (UHB) and the full lower Hubbard band (LHB)) is much smaller than

Δ (the charge-transfer gap), it causes the oxygen non-bonding 2p band to be located in the metal LHB, allowing electrons to only come from LHB during the OER process (Fig. 4a).[43] Transition metal cations of perovskite oxidized species act as active sites and redox centers for intermediates in the adsorption reaction, thus following AEM in the OER process. WIen U is much larger than Δ, the gap is going to be a charge transfer type. The 2p band of oxygen provides electrons, and under applied potential conditions, the non-bonded 2p band of oxygen crosses the Fermi level. The oxygen site will act as a redox center and an LOM-based electron transport pathway may be triggered. For example, by doping with some foreign ion, either the transition metal ion at the B-site or an ion at the A-site.[32,44,45] On the other hand, AEM and LOM can be realized in a class of materials by adjusting defect content or introducing lattice stress while keeping the chemical composition of materials unchanged. Perovskite oxides have high structural tolerance, resulting in a wide range of adjustment of metal 3d and oxygen 2p band structure. Shao-Horn, Stevenson and Xu and colleagues have
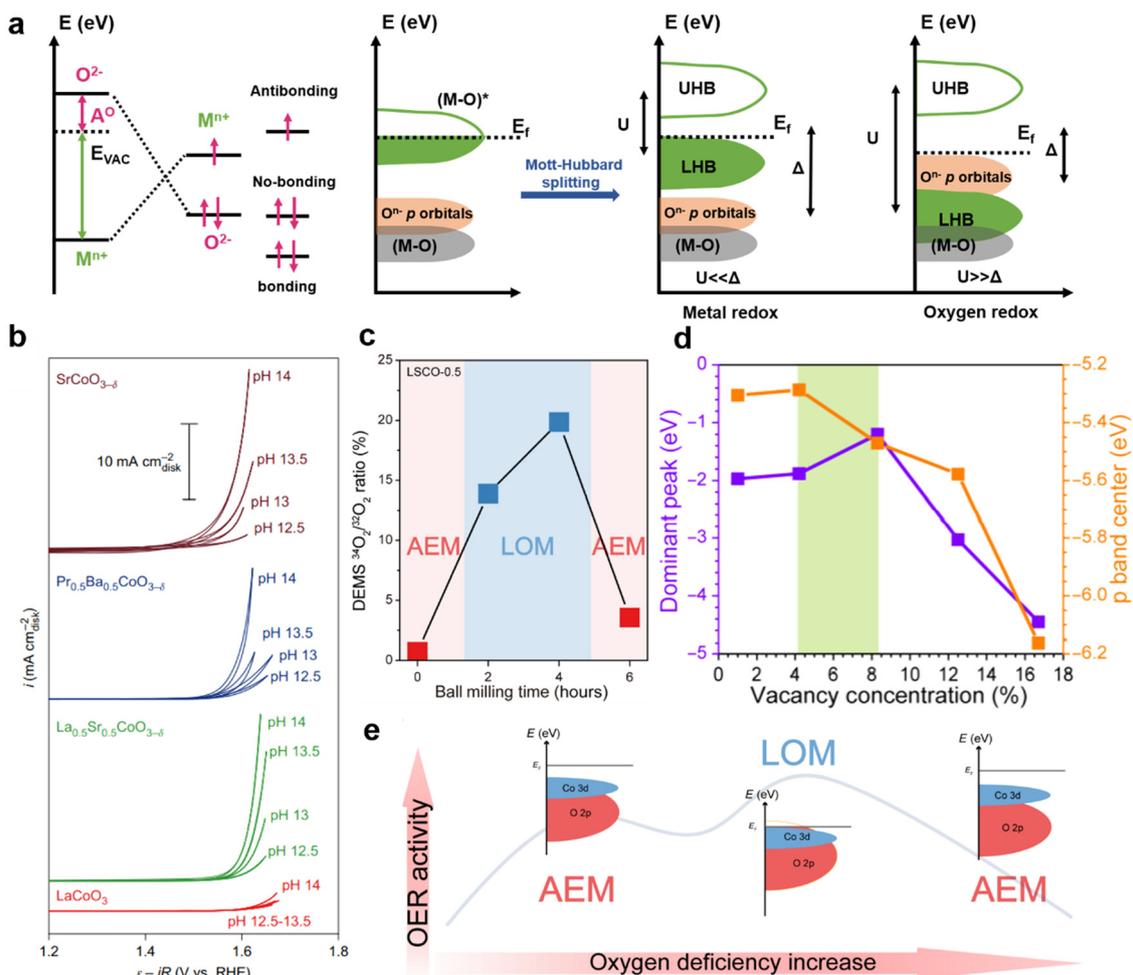

Fig. 4 (a) Schematic descriptions of two possible band structures of perovskite oxides under different oxygen evolution reaction mechanisms. (b) CV measurements from pH = 12.5 to 14 recorded at 10 mV s^{-1}. (c) Effect of ball milling time on different oxygen evolution mechanisms. (d) The dependence of the dominant peak of the p band and the orbital center of the p band on V_O concentration. (e) Transformation of the OER mechanism of oxygen deficiency control and explanation of the structure–activity relationship. Reproduced with permission.[38] Copyright 2022, American Association for the Advancement of Science.

successfully implemented AEM or LOM in different perovskite oxides. The disordered structure can be introduced into perovskite-type catalysts by ball milling and electrical activation to control oxygen defects (Fig. 4b).[32,34,40] This process is usually accompanied by dynamic reconfiguration, and the operation of the LOM mechanism can be judged by whether it depends on the pH of the electrolyte. By cleverly controlling oxygen defect content, Chun-Hua Ya et al. found that the dominant OER mechanism on $La_xSr_{1-x}CoO_3$ can be arbitrarily converted between AEM–LOM–AEM, accompanied by the changing trend of volcanic activity (Fig. 4c–e).[38] By doping other metal ions at the A-site, ball milling, electrical activation and other ways to activate lattice oxygen to adjust oxygen hole concentration, so as to achieve the purpose of mechanism conversion. The synergistic optimization of catalyst activity and stability can be realized by changing the mechanism. In conclusion, the difficulty of cationic and anionic redox reactions in the OER potential region determines which catalytic mechanism is used, thus affecting the performance and behavior of OER catalysts.

3. Catalytic activity descriptors for perovskite oxides

Several OER activity descriptors have been developed over the past few decades, including free energy of adsorbent, e_g occupancy, and metal–oxygen covalence which have the effects of the d-band center and O 2p-band center.

The free energy of adsorbent (ΔG_{ads*}) obtained by theoretical calculation is also a very important descriptor. The catalytic activity of perovskite oxides is strongly influenced by their surface properties, which are determined by their ΔG_{ads*}. In the context of catalysis, it determines the ability of a material to bind and activate reactant molecules, such as H_2O, and facilitate their transformation into product molecules, such as O_2. In general, perovskite oxides with a higher ΔG_{ads*} of water molecules have been found to exhibit higher catalytic activity for the OER (Fig. 5a).[46] However, excessively high ΔG_{ads*} can also result in strong binding of water molecules to the surface, leading to kinetic limitations and decreased catalytic activity. Man et al. considers 18 classes of perovskite and plots η_{OER} as a function of $\Delta G_{O*}-\Delta G_{OH*}$, thus obtaining the universal volcanic relationship.[29] In summary, ΔG_{ads*} of water molecules on the surface of perovskite oxides is an important factor that determines their catalytic activity in the OER, with an optimal range that balances binding strength and kinetic accessibility for efficient conversion of water into oxygen.

OER activity generally depends on oxygen binding strength. The Shao-Horn group proposed that e_g filling of surface transition metal cations (B-site cations) can greatly affect the binding of the OER intermediate and oxide surface, thus affecting the activity of OER. The 3d orbital of the B-site ion in perovskite is hybridized with the 2p orbital of the O. There is a high spatial overlap between the d_{z_2} and $d_{x_2-y_2}$ orbitals in the transition metal and the 2p of oxygen to form σ orbitals. The d_{xy}, d_{yz} and
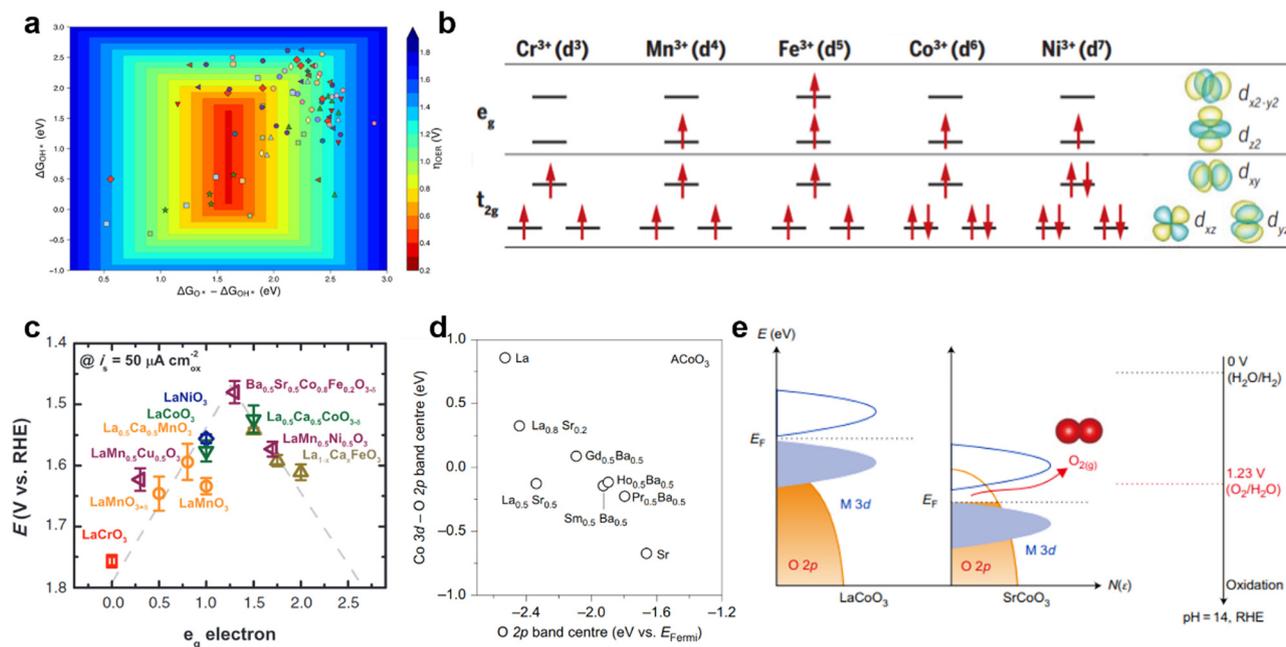
Fig. 5 (a) Two-dimensional OER activity plot of theoretical overpotentials (η_{OER}) for all the materials explored in this study as a function of $\Delta G_{O*}-\Delta G_{OH*}$ and ΔG_{OH*}. Reproduced with permission.[46] Copyright 2020, American Chemical Society. (b) The electronic configuration of some transition metals and related metal orbitals. Reproduced with permission.[17] Copyright 2017, American Association for the Advancement of Science. (c) The relationship between the OER catalytic activity and the occupancy of the e_g-symmetry electron of the transition metal (B in ABO$_3$). Reproduced with permission.[39] Copyright 2011, Science. (d) The difference between the Co 3d band center and O 2p band center and O 2p relative to the Fermi level in ACoO$_3$ perovskites with different A-site cations. (e) Schematic representation of M 3d-O 2p overlap. Reproduced with permission.[32] Copyright 2017, Nature Publishing Group.

d_{xz} metal orbitals have low spatial overlap with oxygen to form π orbitals. The anti-bonding orbitals $\sigma*$ and $\pi*$ are called e_g and t_{2g} orbitals of the octahedral coordination field, respectively. The number and spin state of d-electrons of B-site metal ions affect the filling state of e_g. For example, the filling state of e_g for Cr^{3+}, Mn^{3+}, Fe^{3+}, Co^{3+}, and Ni^{3+} correspond to 0, 1, 2, 1, and 1, respectively (Fig. 5b).[17] Electron transfer between surface cations and adsorption intermediates can be facilitated more directly because the e_g orbital overlaps more strongly with the oxygen-associated adsorbent than the t_{2g} orbital. Therefore, a Shao-Horn (SH) principle with e_g track filling as the activity descriptor is proposed.[39] According to the principle of Shao-Horn (SH), the performance of an oxygen evolution catalyst can be optimized by adjusting the e_g orbital filling of the metal site. They found that the e_g orbitals of $Ba_{0.5}Sr_{0.5}Co_{0.8}Fe_{0.32}O_3$ (BSCF) surface transition metal ions will participate in bonding with surface adsorbed anions *via* σ bond, resulting in significantly higher OER intrinsic activity than IrO_2. This strategy of doping other metal cations at the B-site to regulate e_g orbital filling has been applied by others to achieve better oxygen evolution performance, including $Ca_2Mn_2O_5$, $CaCu_3Fe_4O_{12}$, $SrNb_{0.1}Co_{0.7}Fe_{0.2}O_{3-\delta}$, and $Ca_{0.9}Yb_{0.1}MnO_{3-\delta}$. This descriptor captures the energy variation of the electrochemical OER from the perspective of molecular orbital theory, leading to the formulation of unique OER activity design principles (Fig. 5c). In other words, when surface transition metal ions such as e_g orbital filling ≈ 1, the perovskite oxide catalyst has better catalytic performance.

The relative distance between the band center of the metal 3d (M 3d) and oxygen 2p (O 2p), the covalency of M–O, can be used as a descriptor of catalytic activity. The covalence of M–O bonds in perovskite-type oxides containing various metal ions has an important effect on their catalytic activity and stability.[47] The smaller the relative distance between the M d-band center and O 2p-band center, the stronger the covalent bond of perovskite oxide. Suitable covalent strength can accelerate the charge transfer barrier between metal and oxygen, thus promoting OER properties. But too high covalence will lead to the instability of the catalyst.[48] For AEM, first of all, the increase of covalence leads to an increase in electron density at the metal

site and the decrease of binding energy between the metal site and the oxygen intermediate species.[49] Moreover, the binding energy is adjusted by doping and the length of the M–O bond is changed. The covalency is enhanced and the bond length is reduced, which promotes the formation of oxygenophilic intermediates. In addition, the enhanced M–O covalence will increase the efficiency of charge transfer and reduce the electron charge transfer impedance of perovskite oxide catalysts in the OER process.[50] For LOM, the intensity M–O covalency may cause the O 2p center to shift towards higher energies relative to the Fermi level (Fig. 5d). The location of the center of the O 2p band affects the energy required to form oxygen vacancies.[45] Perovskite oxides with a higher O 2p band center are more likely to form oxygen holes and activate lattice oxygen, which is conducive to improving OER performance. It has also been proved that when M–O bond covalence is enhanced, the contribution of O 2p at the Fermi level is enhanced as a new catalytic center. Yang Shao-Horn *et al.* also proved by DFT that when La^{3+} is replaced by Sr^{2+} at the A-site, the Fermi level is closer to the calculated O 2p band center, which is accompanied by a decrease in the energy gap between the metal 3d and O 2p band center (Fig. 5e).[32] Compared to $LaCoO_3$, the O 2p state of the Fermi level of $SrCoO_3$ is higher than the redox energy of the O_2/H_2O, making the oxidation of lattice oxygen in perovskite more thermodynamically favorable.

4. Engineering of the surface and structure of perovskite oxides

Due to the low conductivity, small number of active sites and slow reaction kinetics, the electrocatalytic activity of the original pure perovskite oxides is not ideal. Therefore, various strategies have been used to improve the electrocatalytic performance of perovskite oxide systems (Table 1). In order to compare the relative activity of the catalyst, the overpotential required to produce a current density of 10 mA cm^{-2} is usually used as the evaluation index (the current density of the solar water splitting device with an efficiency of 12.3%). When the

Table 1 Summary of OER overpotentials at 10 mA cm^{-2} for perovskite oxide-based electrocatalysts

Electrocatalyst	Overpotential [mV *vs.* RHE]	Tafel slope [mV dec^{-1}]	Electrolyte	Loading [mg cm^{-2}]	Electrode	Ref.
$La_{1-x}Ce_xNiO_3$	270	45	1 M KOH	0.4	Carbon paper	22
Ce doped $LaCoO_3$	390	112	1 M KOH	0.25	Glassy carbon	55
$La_{1-x}Sn_xNiO_{3-\delta}$	345	74	1 M KOH	0.367	Glassy carbon	59
$La_{1-x}Sr_xCoO_3$		85	1 M KOH	0.25	Glassy carbon	51
La_2NiMnO_6	350	58	1 M KOH		Glassy carbon	53
$La_{1-x}FeO_{3-\delta}$	410	54	0.1 M KOH	0.232	Glassy carbon	65
$PrBa_{0.5}Sr_{0.5}Co_{2-x}FexO_{5+\delta}$	290	69	1 M KOH	0.192	Glassy carbon	66
$SrCo_{0.4}Fe_{0.2}W_{0.4}O_{3-\delta}$	300		1 M KOH	0.232	Glassy carbon	67
$LaFe_xNi_{1-x}O_3$	302	50	1 M KOH		Glassy carbon	52
$F-Ba_{0.5}Sr_{0.5}Co_{0.8}Fe_{0.2}O_{3-\delta}$	280	101.67	1 M KOH	0.255	Rotating disk	68
S-doped $LaCoO_3$	364	126.7	1 M KOH		Glassy carbon	69
$LaFeO_{3-x-\delta}Cl_x$		59	0.1 M KOH		Rotating disk	70
$Sr_3NiFeMoO_{9-\delta}$	260	42.3	1 M KOH	3	Ni-foam	44
$(La_{0.6}Sr_{0.4})(Co_{0.2}[FeMnNiMg]_{0.8})O_3$	320	45	1 M KOH	0.196	Glassy carbon	71
$La(CrMnFeCo_2Ni)O_3$	325	51.2	1 M KOH	2.35	Ni-foam	72

This journal is © The Royal Society of Chemistry and the Chinese Chemical Society 2023

current density is greater than or equal to 10 mA cm^{-2}, the catalyst is considered to have the potential of industrialization.[54]

4.1. Composition design

Due to the unique structural advantages of perovskite, component regulation can be conducted at the A, B, and O site respectively. Doping of elements generally optimizes the crystal structure parameters and adjusts the electronic structure to achieve the best performance of the OER.

4.1.1. A-site substitution.
A-site element doping can promote the B-site transition metal reconstruction in perovskite OER catalysts. The electronic structure of perovskite oxide can be optimized by using the A-site management method of element substitution engineering. Based on *in situ* electrochemical Raman techniques, Yue Zhang *et al.* found that precise A-site Ce doping in LaNiO$_3$ promotes faster dynamic reconfiguration of the self-assembled NiOOH active layer in the OER process (Fig. 6a).[22] The Co^{3+} spin state in LaCoO$_3$ changes from a low spin state (LS) to medium spin state (IS) after Ce doping at the A-site, thus enhancing the covalence of Co 3d-O 2p.[55] In order to maintain the charge balance, the valence state of the metal at the B-site will be increased and more oxygen vacancies will be generated. For example, the introduction of a lower oxidation state in perovskite by doping the LaCoO$_3$ with Sr^{2+} effectively promotes the movement of crystal oxygen on the active surface of LaCoO$_3$.[56] Wei Huang *et al.* designed various alkali earth metals (Be, Mg, Ca, Sr and Ba) to be doped in LaCoO$_3$, proving that Ca dopants can change the electronic structure and conductivity of LaCoO$_3$, thus significantly improving the electrocatalytic performance.[57] In addition to the change of valence state, doping of the A-site also optimizes the crystal phase. As the doping amount of Sr increases, the lattice parameters of a, b and c decrease and the crystal phase changes from the rhomboid to cubic phase (Fig. 6b). At the same time, the length of the Co–O bond decreases from 1.933 Å to 1.913 Å. The optimized structure has better OER properties when $x = 0.8$ (Fig. 6c).[51] Moreover, the amount of doped ions at the A-site is also related to the OER performance of the catalyst. Ag in LaCoO$_3$ has the maximum solubility at the A-site of perovskite, and too much Ag will produce other impurity phases, which is not conducive to catalytic reactions. According to DRIFTS studies, A-site doped catalysts have two active centers, including a transition metal at the B-site and oxygen vacancy.[58] However, with the Sn substitution ($x = 0.15$), the oxygen concentration will decrease slightly due to excessive Sn–O bonds preventing the formation of oxygen vacancies. The introduction of Sn at the A-site will distort the structure and facilitate surface reconstruction in favor of the OER.[59]

The doping of other elements at the A-site also affects the reaction mechanism of the perovskite catalyst during the OER. For example, the mechanism of catalytic OER has been shown recently to shift from AEM to LOM, through adjusting the Sr in the La$_{1-x}$Sr$_x$CoO$_{3-\delta}$ system of doping.[32,34,36] Zong-ping Shao *et al.* have provided direct evidence of lattice oxygen in the OER by design of the Si-incorporated SrCo$_{1-y}$Si$_y$O$_{3-\delta}$ system.[32] This strategy of regulating the reaction mechanism through A-site doping provides a new perspective for constructing high performance catalysts of the OER.
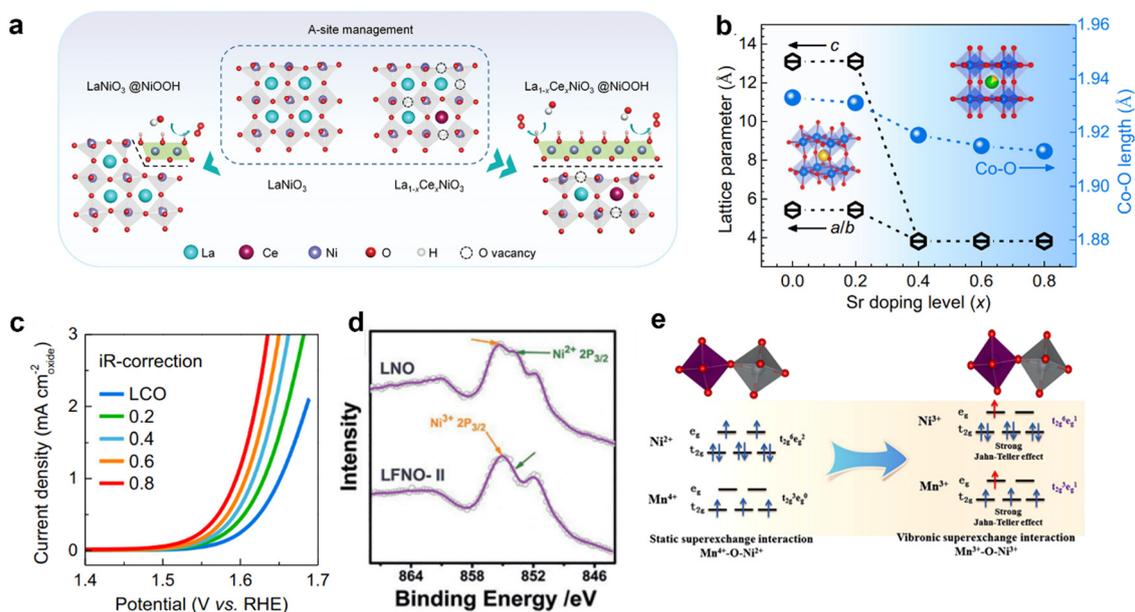
Fig. 6 (a) Schematic diagram of Ce doping accelerated surface reconstruction at site A. Reproduced with permission.[22] Copyright 2021, Wiley-VCH GmbH. (b) The lattice parameters of La$_{1-x}$Sr$_x$CoO$_3$ evolve and the length of the Co–O bond changes with the increase of Sr doped in the A-site. (c) LSV polarization curves with iR-correction of La$_{1-x}$Sr$_x$CoO$_3$ for the OER. Reproduced with permission.[51] Copyright 2021, Elsevier. (d) XPS spectra of Ni 2p$_{3/2}$ for LaFe$_x$Ni$_{1-x}$O$_3$. Reproduced with permission.[52] Copyright 2019, Wiley-VCH Verlag GmbH & Co. KGaA, Weinheim. (e) The influence of electron superexchange between Ni^{3+}–O–Mn^{3+} induces strong Jahn–Teller distortion of MnO$_6$ and NiO$_6$. Reproduced with permission.[53] Copyright 2018, American Chemical Society.

A-site doping also plays a role in improving the stability of catalysts, especially the OER under acidic conditions. Under acidic conditions, the cation in perovskite oxide can easily dissolve into the electrolyte during the OER process, leading to the collapse of the structure.[60,61] The introduction of external cations at the A-site has been reported to improve the activity and stability of ruthenium oxides by preventing or delaying the dissolution of cations. It is found that doping Na^+ in $SrRuO_3$, improves the durability of $SrRuO_3$ perovskite, and maintains 85% of the initial activity after 20 cycles.[62] Higher activity and durability of $Sr_{1-x}K_xRuO_3$ ($x = 0.00, 0.05, 0.10$ and 0.20) can be obtained by partially doped monovalent K^+ cations.[63] The distortion degree of RuO_6 octahedron in perovskite is reduced by doping Na^+/K^+ in $SrRuO_3$. After Na^+/K^+ doping, some Ru cations are oxidized to Ru^{5+}, which reduces the Jahn–Teller effect of Ru^{4+} cations in RuO_6 octahedron.[64] By partially doping Na^+/K^+ at the Sr^{2+} site, $SrRuO_3$ results in an oxide of Ru atoms with higher oxidation states and higher symmetry, thus improving stability. In other words, doping of A-site elements optimizes lattice parameters, leading to improved stability. Moreover, it can adjust the electron distribution state of B-site ions and adjust the covalence of metal - oxygen, thus enhancing the activity for the OER.

4.1.2. B-site substitution. In general, the electrocatalytic activity of perovskites is correlated to B-site doping with transition metals (*e.g.*, Mn,[73] Co,[74,75] Ni,[76,77] and Fe[75,78]) to adopt different valence states and d electron number, which are conducive to the formation of redox couples for the OER process. By doping different metal ions at the B-site and optimizing the corresponding proportion, the electron filling state of e_g for metal was adjusted between the B–O–B′ bond to form more favorable active species for the OER. The doped $SrCoO_3$ perovskites with B-site Fe substitution exhibit a higher catalytic activity than that of pristine BSCF, arising from the surface self-reconstruction to generate more highly-active surface oxyhydroxide species. In spite of this, it is still impalpable to accurately understand the surface self-reconstruction mechanism for more active sites by B-site transition metal substitution in perovskite catalysts.[79] By introducing controlled doping at the B-site to optimize the electron filling state of e_g, excellent OER catalytic performance was obtained in $SrCo_{0.95}P_{0.05}O_{3-\delta}$.[39,80,81] The adjustment of electronic structure and the strong hybridization between O and Ni is achieved by optimizing the Ni/Fe ratio to $8:2$ in $LaFe_xNi_{1-x}O_3$.[52] It is confirmed by *in situ* testing that Ni^{2+}, Ni^{3+}, Fe^{3+} and Fe^{4+} exist in single crystal samples of $LaFe_xNi_{1-x}O_3$, and when Fe replaces Ni, the price of Ni (Fe) will decrease (increase). It can be seen from XPS that the strength of Ni^{2+} is reduced, indicating that the introduction of Fe into $LaNiO_3$ can increase the oxidation state of Ni (Fig. 6d).[52] DFT simulations show the introduction of an additional Fe 3d state near the Fermi level by B-site doping. Electron rearrangement in the Ni–O–Fe bridge strengthens the d-orbital coupling and increases the transition metal (TM) 3d bandwidth, thereby increasing the activity of the OER. In addition, the introduction of other metal ions into the B-site will also affect the lattice structure of the perovskite catalyst. It has been reported that Fe

replaces Ni in epitaxial $LaFe_xNi_{1-x}O_3$ films ($x = 0, 0.125, 0.25, 0.33, 0.375, 0.5,$ and 1.0), resulting in a monotone increase in the out-of-plane lattice parameter (c) with increasing x.

Double perovskites ($A_2BB′O_6$) can also be synthesized by introducing metal ions at the B-site (where the B-site is occupied alternately by different cations B and B′), with the presence of oxygen bridges connecting each B and B′ atom pair.[27,82,83] The coupling effect can be enhanced by adjusting the B–O–B′, providing a basis for tailoring their electronic structure. The ordered arrangement of B-site ions results in a superior physical correlation effect in double perovskites. The e_g electron filling state of metal can be adjusted by optimizing B-site ions. On the other hand, theoretical and experimental studies have proved that doping other ions at the B-site of perovskite oxides can regulate the electron distribution of metal–oxygen bonds and accelerate the formation of active components. For example, the electron super-exchange of Ni^{3+}–O–Mn^{3+} in La_2NiMnO_6 nanoparticles causes the electron filling states of e_g of Mn and Ni ions to become uniform (Fig. 6e).[53] In addition, the electron super-exchange interaction of Ni^{3+}–O–Mn^{3+} induces strong Jahn–Teller distortion of MnO_6 and NiO_6 octahedrons, elongating M–O bonds and contributing to the formation of Mn/Ni hydroxide/oxide active components on the surface of La_2NiMnO_6.[84]

In particular, the electrocatalytic performance of perovskite materials can be improved by adding nonmetallic elements at the B-site. By adding the corresponding salt to the synthesis, P or B can be introduced at the B-site of the lattice.[85] P. R. Slater and co-workers found that the conductivity of $CaMn_{0.95}P_{0.05}O_{3-\delta}$ and $CaMn_{0.95}B_{0.05}O_{3-\delta}$ was significantly improved compared with the original catalysts, which is attributed to the addition of O_2^{2-}/O^- and the optimization of electron filling in e_g.[86] Another phosphor-doped perovskite $SrCo_{0.85}Fe_{0.1}P_{0.05}O_{3-\delta}$ (SCFP) has been reported to stabilize the crystal structure of the oxide by introducing P. In addition, it has been reported that silicon-doped perovskite can stabilize the cubic structure and enhance the ionic conductivity of perovskite, such as $SrM_{1-x}Si_xO_3$ (M = Fe, Mn, Co), $Ba_2In_{2-x}Si_xO_{5+x/2}$ ($x = 0, 0.1, 0.2, 0.3$).[87–89] Therefore, the addition of nonmetallic elements to the B-site of perovskite oxides opens up a new field for the design of high-performance and stable oxygen evolution catalysts.

4.1.3. Oxygen-site substitution. The introduction of other ions at the O-site can modify the O 2p-band center (valence electrons in the p orbital), providing new opportunities to adjust the properties of perovskite oxides. From the point of view of charge compensation, the partial substitution of O^{2-} by a negatively charged anion (F^-, Cl^-) may produce O^{2-}/O^-, which can enhance the activity of the OER. When F^- is introduced into $La_{0.5}Ba_{0.5}CoO_{3-\delta}$, the upper bound of the bonding orbital is close to the Fermi level, which reduces the charge transfer energy barrier of electrocatalysis (Fig. 7a). It is calculated that the energy barrier of $La_{0.5}Ba_{0.5}CoO_{2.9-\delta}F_{0.1}$ (0.270 eV) is even lower than that of active β-CoOOH (0.48 eV) due to the trapping of electrons by F^- in neighboring atoms. F^- is highly electronegative, allowing OO* to be released more easily, resulting in a more efficient OER performance.[90] In $Ba_{0.5}Sr_{0.5}Co_{0.8}Fe_{0.2}O_{3-\delta}$, O^{2-} is partially replaced by F^- to form

the M–F–M (M = Co or Fe) ligand. The current density of $Ba_{0.5}Sr_{0.5}Co_{0.8}Fe_{0.2}O_{3-\delta}$ with 1% F atomic ratio is 68 mA cm^{-2} about 3.5 times that of IrO_2 at 1.63 V for the OER. Appropriate F^- substitution can improve the performance for the OER. When the concentration of F-is excessive, O^{2-}/O^- species will be consumed because the Me–O–M bond will be replaced by two M–F bonds, which is not conducive to the reduction of B-site cations and the production of O^{2-}/O^- (Fig. 7b and c).[68] Through first-principles calculations, D. Gao et al. first proved that s doping in perovskite oxides can introduce oxygen defects and promote the conductivity of Co^{3+}. At the potential determination step $(O^* + H_2O (l) \rightarrow HOO^* + H^+ + e^-)$, S-doped $LaCoO_3$ with an oxygen defect had the lowest overpotential ($\eta = 1.00$ V), indicating that S doping was the main factor for activating the catalytic behavior of adjacent Co sites (Fig. 7d and e).[69] At the same time, the electron filling of the e_g state of Co^{3+} was adjusted to improve the catalytic performance.[69] The electronegativity of Cl is lower than that of O. The doping of Cl in $LaFeO_{2.9-\delta}Cl_{0.1}$ enhances the covalence of metal–oxygen, which is conducive to the charge transfer in the electrocatalytic process. Surface-sensitive soft X-ray absorption spectroscopy (sXAS) showed that the energy of the Fe L-edge peak of $LaFeO_{2.9-\delta}Cl_{0.1}$ decreased slightly relative to the parent $LaFeO_{3-\delta}$, indicating that the valence state of Fe was reduced by Cl doping (Fig. 7f).[70]

4.2. Morphology engineering

The morphology of perovskite oxide has an important effect on the OER performance. Structures with a larger electrochemically active surface area (ECSA) tend to have more catalytic active sites, which is conducive to enhancing the transport of substances. Morphological engineering has more influence on the catalytic surface. In recent years, perovskite oxides have been developed by researchers with a variety of nanostructures, such as: nanoparticles, nanowires, nanotubes, nanorods, nanospheres and so on. Meso-porous and macro-porous structures were found in $SrNb_{0.1}Co_{0.7}Fe_{0.2}O_{3-\delta}$ perovskite nanorods prepared by electrospinning (Fig. 8a). Compared with the bulk structure, the large pore size distribution range and the increase of pore number are conducive to the exposure of the catalytic active site and the mass transport associated with electrocatalysis, thus showing high efficiency OER activity in alkaline solution.[91] The yolk–shell $La_{0.9}Sr_{0.1}CoO_3$ perovskite microspheres were synthesized using a one pot method. The unique Yolk–Shell $La_{0.9}Sr_{0.1}CoO_3$ perovskite microspheres showed strong catalytic activity for the OER (Fig. 8b).[92] Its structure has advantages: (1) larger ECSA on the unit scale of coarse nanocrystals provides more active sites for the OER; (2) the shorter length is conducive to the diffusion of electrons and oxygen ions, thus speeding up the electrochemical kinetics; (3) the thin hollow structure on the three-dimensional
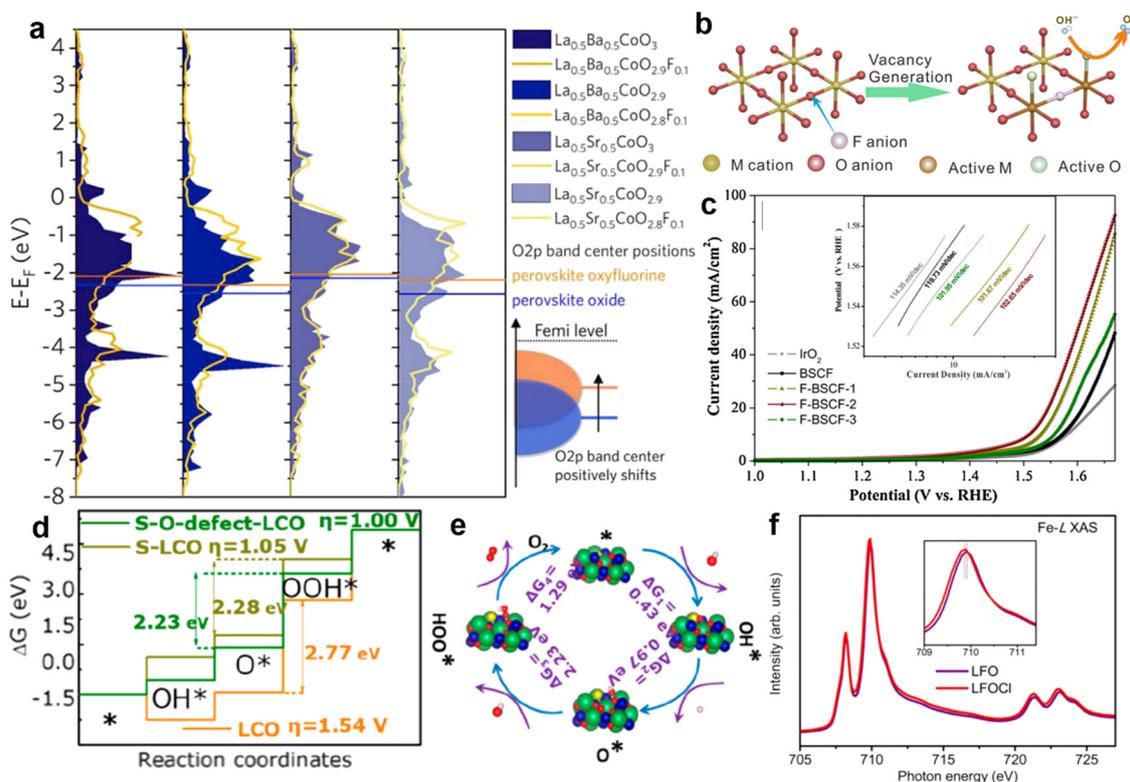

Fig. 7 (a) The density of states (the sum of the upper and lower spin states) in the O 2p band of perovskite oxides with different F doping contents. Reproduced with permission.[90] Copyright 2018, Elsevier. (b) The process by which F replaces O-site atoms to produce O^{2-}/O^- species. (c) LSV diagram regarding different contents of F substitution in $Ba_{0.5}Sr_{0.5}Co_{0.8}Fe_{0.2}O_{3-\delta}$. Reproduced with permission.[68] Copyright 2019, Elsevier. (d) Gibbs free energy variation of $LaCoO_3$ doped with S and oxygen defects in the four steps of the OER. (e) Reaction mechanism of S-doping leading to an oxygen defect of LCO for the OER. Reproduced with permission.[69] Copyright 2020 American Chemical Society. (f) The sXAS spectra of Fe-L for $LaFeO_3$ and $LaFeO_{2.9-\delta}Cl_{0.1}$. Reproduced with permission.[70] Copyright 2020, Elsevier.
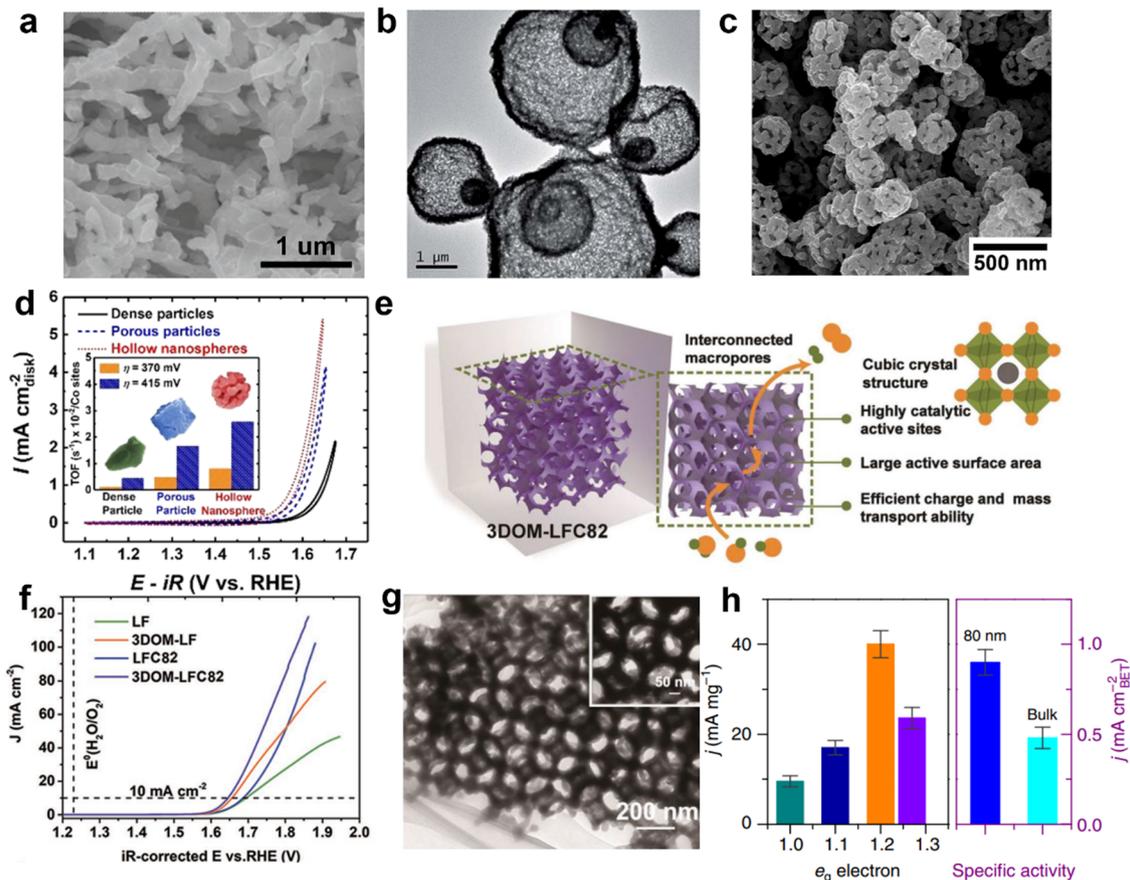
Fig. 8 (a) Scanning electron microscopy (SEM) image of nanorods $SrNb_{0.1}Co_{0.7}Fe_{0.2}O_{3-\delta}$ prepared by electrospinning technology. Reproduced with permission.[91] Copyright 2016 WILEY-VCH Verlag GmbH & Co. KGaA, Weinhei. (b) TEM image of Yolk−Shell $La_{0.9}Sr_{0.1}CoO_3$. Reproduced with permission.[92] Copyright 2015, The Royal Society of Chemistry. (c) SEM images of hollow spheres $LaCoO_3$. (d) CV curves of $LaCoO_3$ with different morphologies for the OER. Reproduced with permission.[93] Copyright 2017, American Chemical Society. (e) Schematic diagram of the advantages of 3D ordered macro-porous electrocatalysts for the OER. (f) LSV curves of various catalysts for the OER. (g) TEM image for 3D ordered macro-porous electrocatalysts. Reproduced with permission.[94] Copyright 2018, WILEY-VCH Verlag GmbH & Co. KGaA, Weinheim. (h) Mass and special activities for nanoparticle catalysts of different sizes at an overpotential = 0.49 V. Reproduced with permission.[95] Copyright 2016, Springer Nature.

(3D) space is conducive to maintaining the integrity of the structure and preventing aggregation or sintering, which is conducive to maintaining a stable structure during the long catalytic process. Hong Yang *et al.* prepared $LaCoO_3$ with porous particles and hollow nanospheres using a hydrothermal method (Fig. 8c). By adding the organic substance glycine to the synthesis as a pore-forming agent, it will spill out in the structure due to high temperature calcination. This makes $LaCoO_3$ with the amorphous surface structure exhibit a low initial potential in OERs (Fig. 8d). The OER performance of $LaCoO_3$ hollow nanospheres ($\sim$1.50 V) is the best compared with that of dense ($\sim$1.55 V) and porous particles ($\sim$1.51 V).[93] Zong-ping Shao *et al.* impregnated a neatly arranged colloidal crystal template of polymethyl methacrylate (PMMA) with a mixed metallic solution (Fig. 8e).[94] Perovskite oxide with a 3D ordered macro-porous structure was obtained by removing the tightly packed spherical template by calcination. Open interconnected 3D ordered macro-porous structures have uniformly distributed pores with an average diameter of about 200 nm, resulting in a high specific surface area, which is conducive to O_2/OH^- transport channels and electron migration

(Fig. 8f, g). Yang's group also prepared sea urchin-like nanostructures with high specific surface area (48 $m^2\ g^{-1}$), which followed the "nucleation-growth-assembly" route.[96] Regulating the nanostructure of perovskite oxides can also affect the electron configuration of active sites. For example, by reducing the particle size, the regulation successfully increased the fill of e_g of Co^{3+} in $LaCoO_3$ from about 1.0 to an optimized configuration close to 1.2.[95] The orbital hybridization of Co 3d-O 2p and the weakening of the Co–O bond favor the formation of –OOH species, thus increasing the intrinsic activity of $LaCoO_3$.[97,98] In addition, by normalized specific activity comparison in the Brunauer–Emmett–Teller (BET) region, the activity of the 80 nm sample is still 1.8 times that of the bulk sample, indicating that the significant enhancement of OER activity is mainly due to the increase of reactivity at the active site, that is, due to the spin state transition of Co^{3+} on the surface (Fig. 8h).[95] The surface regulation of perovskite oxides is more complicated. It can not only increase the exposure of more active sites, but also regulate the internal electron distribution. The influence on oxygen evolution performance has many aspects that need to be further studied and

explored, to provide more basis for the design of catalysts with high performance.

4.3. Defect engineering

The introduction of anion or cation defects in the perovskite structure may regulate the electron distribution and optimize the reaction path, which contributes to the electrocatalytic capacity.

4.3.1. Oxygen vacancy. The concentration of oxygen vacancy affects the electronic structure and valence state of B-site metal cations, thus regulating the M–O covalent bond. In addition, oxygen-deficient perovskite oxides have a large number of oxygen vacancies as a new active adsorption/reaction site, which helps to improve the catalytic activity of the OER. Hong Yang et al. synthesized anoxic $Ca_2Mn_2O_5$ by annealing at low temperature in a gas containing 5% H_2/Ar.[101] Anoxic perovskite $Ca_2Mn_2O_5$ has an orthogonal crystal structure in which oxygen atoms are bonded to adjacent subunits (MnO_5) by angular oxygen atoms. Therefore, $Ca_2Mn_2O_5$ has inherent porosity at the anoxic site at the molecular level, which facilitates ion transport through oxygen vacancies in the OER. The presence of oxygen vacancy in the anoxic structure leads to the large Jahn–Teller effect of $Ca_2Mn_2O_5$, which distorts the anoxic perovskite structure. The introduction of oxygen vacancy changes the electron configuration of Mn^{4+} ($3d^3$, t_{2g}^3) into Mn^{3+} ($3d^4$, $t_{2g}^3 e_g^1$). One electron in manganese with a high spin orbital can form a bonding structure with OH^-, which results in the high OER activity of the anoxic perovskite $Ca_2Mn_2O_5$. The combination strategy of Sr doping and Ar plasma treatment generates more oxygen vacancies as new active sites in $LaCoO_3$ perovskite, thus obtaining excellent OER performance.[102] The perovskite $LaMn_{0.75}Co_{0.25}O_{3-\delta}$ was prepared by a two-step calcination process, with abundant oxygen vacancies in its structure. The OER performance of the obtained anoxic $LaMn_{0.75}Co_{0.25}O_{3-\delta}$ was 27.3 times that of the untreated $LaMn_{0.75}Co_{0.25}O_3$ and comparable to that of the commercial RuO_2.[103] The increase of tensile strain also leads to the increase of oxygen vacancy content in $NdNiO_3$

films. Oxygen vacancy can reduce Ni^{3+} to Ni^{2+} with adjustment of the average occupancy of e_g, thus increasing the activity for the OER. The transformation of strain state induces lattice distortion and defects, which is conducive to the activity of the OER.[104] In the highly oxidized water environment, the anoxia in $SrCoO_{3-\delta}$ film was artificially adjusted from $\delta \leq 0.1$ to $\delta \sim 0.25$ by changing the epitaxial strain of the $SrCoO_{3-\delta}$ film, which significantly enhanced the OER activity.[105] Moreover, lattice distortion can be generated by substituting the B-site with valence exchange element gradient and constructing different interfaces, so as to optimize the surface oxygen vacancy concentration of rare-earth base perovskite oxides, thus improving the catalytic activity.[106,107] Sean C. Smith et al. believed that excessive oxygen vacancy near Co as the active site would reduce its catalytic activity. The reason may be that the oxygen vacancy in $SrCoO_3$ donates two electrons in the form of a local charge to the adjacent Co site. The first-principles calculation shows that the formation energy and migration energy of a single vacancy are about 1.26 eV and 0.5 eV. Under the premise of ensuring the OER activity of the material, the surface oxygen vacancy formation energy can be increased by about 30% by adjusting the moderate biaxial compression strain (2%), thus reducing the surface vacancy concentration (Fig. 9a).[99] The energy of perovskite surface reduction (and oxidation) is different from that of the bulk, resulting in the formation of an oxygen vacancy on the perovskite surface more easily than the bulk. William C. Chue et al. found that surface lattice oxygen anions are also key partners in the redox of oxygen molecules, in addition to the redox of transition ions.[108]

Among the several mechanisms proposed for the LOER is the involvement of active sites for oxygen evolution by oxygen, resulting in the creation of surface oxygen vacancies. In other words, there is a perovskite catalyst with a high oxygen vacancy content and oxygen may occur through the LOM. The ability of $PrBaCo_2O_{5+\delta}$ to accommodate a wide range of oxygen vacancies makes it an excellent candidate for studying oxygen vacancies. Emiliana Fabbri et al. systematically studied the increase of
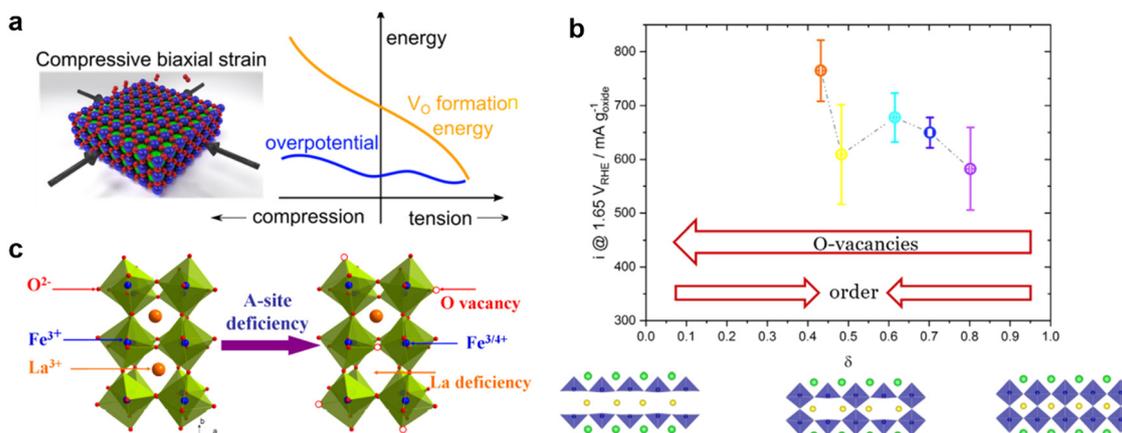
Fig. 9 (a) Schematic diagram of the effect of compressive strain and tension strain on OER overpotential and oxygen vacancy formation energy. Reproduced with permission.[99] Copyright 2016, American Chemical Society. (b) OER activity of $PrBaCo_2O_{5+\delta}$ in different oxidation stoichiometry. The structure diagrams below show the distribution of oxygen vacancy in the structure of PBCO with δ = 0, 0.5 and 1. Reproduced with permission.[100] Copyright 2021, Wiley-VCHGmbH. (c) Schematic diagram of the formation of oxygen vacancy and Fe^{4+} in $La_{1-x}FeO_{3-\delta}$ perovskite with A-site deficiency. Reproduced with permission.[65] Copyright 2016, American Chemical Society.

OER activity in $PrBaCo_2O_{5+\delta}$ materials with the increase of lattice oxygen vacancy. However, the relationship between OER activity and oxidation stoichiometry is not linear (Fig. 9b). When $\delta \approx$ 0.5, $PrBaCo_2O_{5+\delta}$ forms alternating $[CoO_6]$ octahedrons and $[CoO_5]$ square pyramids in the plane of Pr. This arrangement of oxygen vacancies causes significant changes in Co–O coordination and Co–O plane buckling, which is detrimental to the OER activity of perovskite.[100] In general, the reduction atmosphere can be maintained during synthesis, physical treatment (Ar plasma treatment, biaxial compression/tension strain), or A/B site elements can be doped to form oxygen vacancies in perovskite oxides. The presence of an appropriate amount of oxygen vacancy regulates crystallographic characteristics, rearranges electron distribution and optimizes adsorption energy, thus achieving excellent performance for the OER.

4.3.2. Cation vacancy. The A-site cationic vacancies can cause oxygen vacancies and regulate the B-site filled e_g orbitals to further improve the catalytic activity of the OER. Zong-ping Shao et al. constructed the first highly efficient bifunctional catalyst $La_{1-x}FeO_{3-\delta}$ ($x = 0.02, 0.05, 0.1$) by simply introducing a cationic deficiency at the A-site. $La_{0.95}FeO_{3-\delta}$ showed the best activity for the ORR and OER. The high activity of $La_{0.95}FeO_{3-\delta}$ can be attributed to the formation of many oxygen vacancies and few Fe^{4+} species on the surface of perovskites due to cationic vacancies (Fig. 9c).[65] The crystallography parameters of perovskite oxides can be changed by A-site vacancy. The absence of A-site for $(La_{0.8}Sr_{0.2})_{1-x}Mn_{1-x}Ir_xO_3$ will generate oxygen vacancies and reduce the valence state of B-site metal ions, leading to lattice expansion. Compared with $La_{0.8}Sr_{0.2}MnO_3$ ($a = 5.453$ Å, $b = 5.504$ Å, $c = 7.761$ Å), the lattice parameters of $(La_{0.8}Sr_{0.2})_{1-x}Mn_{1-x}Ir_xO_3$ ($a = 5.460$ Å, $b = 5.501$ Å, $c = 7.769$ Å) are larger. Partial reduction of the valence state of the B-site metal cation (Mn) makes the metal–OH bond weaker, while more oxygen vacancies enhance the electrochemical performance for the OER.[109] The percentage of Mn^{4+} increased in $(La_{1-x}Sr_x)_{0.98}MnO_3$ ($x = 0.2, 0.3, 0.4$ and 0.5) compared to $La_{1-x}Sr_xMnO_3$. At the Fermi level, the spectral region of about 3.61 eV shows a large increase in intensity, indicating enhanced Mn 3d-O 2p hybridization. This indicates that the addition of A-site cation vacancies can not only regulate the valence state of Mn, but also optimize the oxygen adsorption capacity of catalyst.[110] The current density of A-site cation-deprived $(Ba_{0.5}Sr_{0.5})_{1-x}Co_{0.8}Fe_{0.2}O_{3-\delta}$ is about 56% higher than that of fully oxidized $Ba_{0.5}Sr_{0.5}Co_{0.8}Fe_{0.2}O_{3-\delta}$ at 1.7 V (vs. RHE). Experimental studies have shown that the higher surface oxygen vacancy associated O_2^{2-}/O^- content of $(Ba_{0.5}Sr_{0.5})_{1-x}Co_{0.8}Fe_{0.2}O_{3-\delta}$ oxide leads to a faster charge transfer rate, thus enhancing the OER activity. DFT results show that the O 2p band center of perovskite with an A-site cation defect is closer to the Fermi level.[111] Perovskite oxide with a double cationic defect at the A-site was prepared by an improved molten salt method. The introduction of double-cationic defects at the A-site can coordinate the production of oxygen vacancies in $La_{0.6}Sr_{0.4}Co_{0.8}Fe_{0.2}O_{3-\delta}$ and the oxidation state of elements at the B-site. In order to maintain charge neutrality, the oxidation state of cations at the B-site increases and oxygen vacancies exist.

However, excessive double-cation vacancies at the A-site are not conducive to maintaining the crystal structure of perovskite. This can be attributed to the fact that when there are too many cationic vacancies at the A-site to be sufficient for the coordination to form impurity phases from dissolved B-site metals. Therefore, it is the key to construct efficient perovskite oxides for the OER without damaging the structure of perovskites by introducing cationic defects.[112]

5. Noble-perovskites for the OER in acidic media

Recently, a proton exchange membrane water electrolyser (PEMWE) with high current density (maximum 2–3 A cm^{-2}) and ultrahigh gas purities has become a commercial or near-commercial electrochemical water cracking technology.[113–115] However, PEMWEs require the use of noble metal based electrocatalysts in the anode, such as iridium (Ir), ruthenium (Ru) or their oxide forms. The high cost and scarcity of Ir and Ru limit the large-scale application of PEMWE, but the instability of some non-noble metal catalysts in strongly acidic solutions makes their electrocatalytic OER activity lower than that of noble-metal based materials. Therefore, it is necessary to develop noble metal OER electrocatalysts with high electrocatalytic activity and good stability in acidic solutions. One of the more direct approaches is to develop catalysts with lower noble metal content while ensuring high performance. Perovskite oxide is a candidate for acid catalysts because it can be doped with multiple metal elements at the A/B-site (Table 2). The OER process of Ir/Ru-based perovskite oxide is often accompanied by the dissolution of elements, which not only affects the structure, but also forms a new catalytic surface.

5.1. Ir-based perovskites

Jaramillo and co-workers prepared a catalyst composed of $SrIrO_3$ epitaxial thin films by pulsed laser deposition.[116] Sr was leach from the surface layer of $SrIrO_3$ film to form a highly active surface layer IrO_x, which improved the activity of the catalyst in the stability test held at 10 mA cm_{geo}^{-2} (current normalization to the geometric surface area of the electrode) in 0.5 M H_2SO_4. An overpotential of 340 mV is required for the initial $SrIrO_3$ to reach 10 mA cm_{geo}^{-2}. After the current density of 10 mA cm_{geo}^{-2} was maintained for 10 minutes, the overpotential decreased to 320 mV. After 2 hour constant-current tests, $IrO_x/SrIrO_3$ only required 270 mV of overpotential to reach 10 mA cm_{geo}^{-2}. DFT calculations were performed to further understand the production of active species on the surface of $SrIrO_3$ (Fig. 10a and b). The theoretical overpotential is calculated for the possible generation of various overburden structures, IrO_2-anatase, anatase $IrO_2(001)$, IrO_2-sheets, IrO_3, rutile $IrO_2(110)$, rutile $IrO_2(100)$, on $IrO_x/SrIrO_3$ surfaces with Sr defects (Fig. 10b). Studies have shown that the formation of IrO_3 or anatase IrO_2 sites may be stable and active overlay structures, but the presence of other more active species cannot be excluded. In other words, dissolution of IR-based perovskite

This journal is © The Royal Society of Chemistry and the Chinese Chemical Society 2023

Table 2 OER performance (activity and durability) in acid electrolyte for state-of-the-art Ir/Ru-based perovskite oxide catalysts

Electrocatalyst	Overpotential [mV vs. RHE]	Durability tests	Electrolyte	Loading [mg cm^{-2}]	Ref.
Ba_2YIrO_6	340	1 h @j = 10 mA cm^{-2}	0.1 M HClO$_4$	0.015	12
$IrO_x/SrIrO_3$	270–290	30 h @j = 10 mA cm^{-2}	0.5 M H$_2$SO$_4$		116
$IrO_x/9R$-$BaIrO_3$	230	48 h @j = 10 mA cm^{-2}	0.5 M H$_2$SO$_4$	0.283	118
$6H$-$SrIrO_3$	248	30 h @j = 10 mA cm^{-2}	0.5 M H$_2$SO$_4$	0.90	117
$Sr_{0.9}Na_{0.1}RuO_3$	170		0.1 M HClO$_4$	0.51	62
$CaCu_3Ru_4O_{12}$	171	24 h @j = 10 mA cm^{-2}	0.5 M H$_2$SO$_4$	0.25	121
$Cr_{0.6}Ru_{0.4}O_2$	175	10 h @j = 10 mA cm^{-2}	0.5 M H$_2$SO$_4$	0.283	122
$W_{0.2}Er_{0.1}Ru_{0.7}O_{2-\delta}$	167	500 h @j = 10 mA cm^{-2}	0.5 M H$_2$SO$_4$	0.33	18
$SrTi_{1-x}Ir_xO_3$	247	20 h @j = 10 mA cm^{-2}	0.1 M HClO$_4$	0.21	123
Sr_2IrO_4	286	6 h @j = 10 mA cm^{-2}	0.1 M HClO$_4$	0.08	124
Sr_4IrO_6	287	6 h @j = 10 mA cm^{-2}	0.1 M HClO$_4$	0.08	124

oxides tends to occur in acidic OERs. How to expose more active sites in a way that minimizes dissolution and reconstitution is the key question. Xiao-xin Zou *et al.* studied Sr_2IrO_4 of the Ruddlesden–Popper phase, which has unique structural
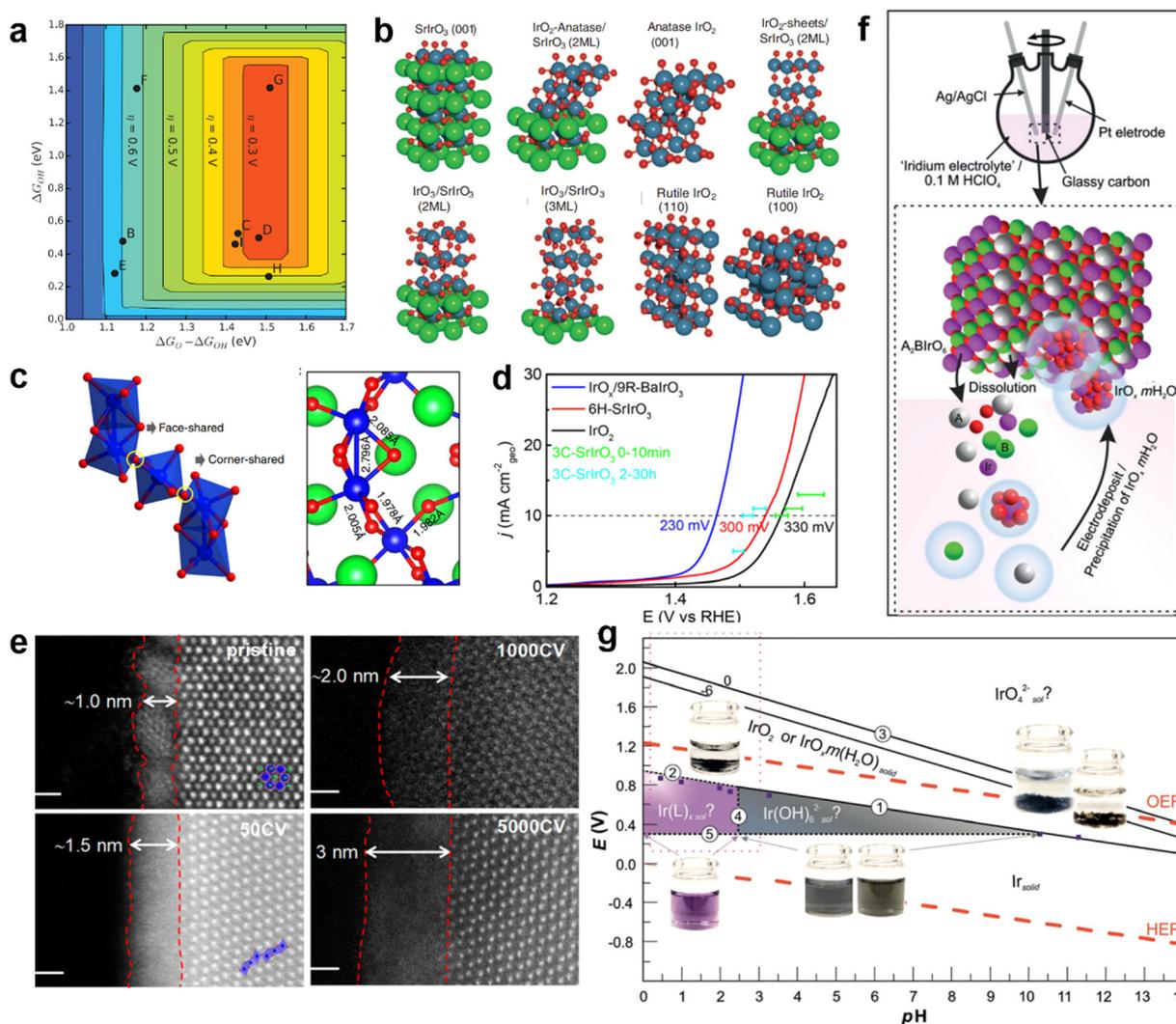
Fig. 10 (a) The theoretical overpotential of IrO$_x$ with different structures exists on the surface with O* and OH* binding energies as the descriptor. (b) The model of the surface of IrO$_x$ with different structures. Reproduced with permission.[116] Copyright 2016, American Association for the Advancement of Science. (c) Crystal structure of 6H-SrIrO$_3$ and different connection modes of IrO$_6$ octahedron. Reproduced with permission.[117] Copyright 2018, Sprinter Nature. (d) LSV curves of IrO$_x/9R$-BaIrO$_3$, IrO$_2$, and 6H-SrIrO$_3$ in 0.5 M H$_2$SO$_4$. (e) HAADF-STEM image of the IrO$_x/9R$-BaIrO$_3$ surface after a CV test with different times. Reproduced with permission.[118] Copyright 2021, American Chemical Society. (f) The proposed OER catalytic mechanism in Ir-based perovskite oxidation species involves iridium dissolution-electrodeposition. (g) Iridium E_H–pH diagram. Reproduced with permission.[119] Copyright 2019, Wiley-VCH.

advantages: (1) the interlayer Sr^{2+} can be exchanged with protons in a controlled manner while keeping the perovskite structure unchanged; (2) protonated layered perovskite can be stripped into nanosheets with a higher surface area and more active sites. Iridium nanosheet structures were obtained by liquid phase stripping with interlayer channels that prevented electron transfer between the inner and outer Ir atoms, thus reducing the charge density around the Ir sites outside the surface.[120] It regulates the ability of the Ir site to bind oxygen intermediates and improves OER activity. Xiao-xin Zou et al. found that 6H-SrIrO$_3$ had 27.1 wt% less iridium than IrO$_2$, but 6H-SrIrO$_3$ had almost 4 times the OER activity of IrO$_2$ at 1.525 V. The crystal structure of 6H-SrIrO$_3$ was still maintained after 48 days of exposure in strong acidic medium (0.5 M H$_2$SO$_4$).[117] Moreover, Ir species were not detected in acidic solution, indicating that 6H-SrIrO$_3$ has good durability in acidic environments. The results of DFT simulations show that the surface of 6H-SrIrO$_3$ with Ir atoms in a face-sharing octahedral dimer has better catalytic activity than the surface of 6H-SrIrO$_3$ with Ir atoms in an isolated horn-sharing IrO$_6$ octahedron for the OER (Fig. 10c). Yan and co-workers studied 9R-BaIrO$_3$ with 1nm surface IrO$_x$ nanoparticles (IrO$_x$/9R-BaIrO$_3$).[118] Its iridium mass activity (168 A g$_{Ir}^{-1}$) is about 16 times higher than that of IrO$_2$ (10 A g$_{Ir}^{-1}$) in acidic OERs (Fig. 10d). The structure of the active layer on the surface of IrO$_x$/9R-BaIrO$_3$ evolved during the acidic OER process. During the acidic OER process, the valence state of Ir changes, in which the final surface contains a high content of the high valence state Ir^{5+}O$_x$. The crystal morphology of the catalyst also evolved from the initial nanoparticle crystal to amorphous octahedron (Fig. 10e). The willingness of IrO$_x$/9R-BaIrO$_3$ to have excellent acidic activity of the OER can be attributed to the formation of a large amount of high-valence amorphous iridium oxide on the surface and strong metal conductivity.[118]

According to the research, a small amount of Ir will be dissolved in a strongly acidic environment, and then deposited on the surface of the catalyst in the form of oxides (IrO$_x$·mH$_2$O). The behavior of Ir-based perovskite oxides in the OER can be summarized as solution-electrodeposition of iridium species (Fig. 10f). The behavior of Sr$_2$FeIr(v)O$_6$ and Sr$_2$Fe$_{0.5}$Ir$_{0.5}$(v)O$_4$ in acidic OER was studied using CV. The estimated precipitation potential is E_{p-IrOx} = 0.92 V (vs. RHE). In other words, electrodeposition occurs when the applied external potential exceeds the precipitating potential of IrO$_x$·mH$_2$O. This re-deposition of Ir species from the perovskite structure onto the catalyst surface to form IrO$_x$·mH$_2$O is correlated with the applied potential, which follows the Pourbaix diagram of iridium.[119] Moreover, the OER activity of Ir-based perovskite oxides is also constrained by a stable potential/pH domain.

Alexis Grimaud et al. reconstructed E_H-pH maps of iridium based on their experimental results and the equation established by Pourbaix, thus further discussing the existence forms of Ir species in different potential and electrolyte environments (Fig. 10g).[119] E_{p-IrOx} was used as the critical potential for distinguishing soluble iridium in solids IrO$_x$·mH$_2$O and IrO$_2$. Ir-based perovskites, such as Sr$_2$CoIr(v)O$_6$, La$_2$LiIr(v)O$_6$, Ba$_2$PrIr(v)O$_6$ and

Ba$_2$LaIr(v)O$_6$, have higher open circuit potentials than E_{p-IrOx}. When exposed to low pH, these perovskite iridium species precipitate to IrO$_x$·mH$_2$O as OER active species under their open-circuit voltage.

5.2. Ru-based perovskites

Like Ir-based perovskite oxides, Ru-based perovskite oxides also dissolve or are more easily dissolved in acidic environments, which is the reason why Ru-based perovskite oxides have been less studied in acidic OER. Schmidt et al. prepared SrRuO$_3$ nanoparticles using a simple flame spray synthesis method.[61] The thermodynamically stable phases of Sr$_2$Ru$_3$O$_{10}$, Sr$_4$Ru$_2$O$_9$, Sr$_2$RuO$_4$ and SrRuO$_3$ were explored by adjusting the different proportions of Sr and Ru during synthesis. In acidic environments, perovskite oxides undergo an OER process accompanied by dissolution at an oxidation potential (ABO$_3$ + 2H$^+$ ↔ A^{2+} + BO$_2$ + H$_2$O). RuO$_2$ easily forms RuO$_2$(OH)$_2$ and further RuO$_4$. Therefore, the high current response of Ru-based perovskite oxide materials in an acidic environment may be due to the OER and Ru corrosion. Studies of SrRuO$_3$ films using a rotating ring disk electrode with ruthenium platinum rings, where the measured currents were attributed to the OER (90%) and Ru corrosion (10%). In the Pourbaix diagram of SrRuO$_3$, it is found that SrRuO$_3$ is easily decomposed by chemical dissolution in any aqueous solution (Fig. 11a).[61] As a result, SrRuO$_3$ has difficulty maintaining the perovskite structure in applications involving contact with water-based solutions (mainly involving the OER). The instability of the SrRuO$_3$ structure is due to the dissolution of Sr^{2+} in most pH domains within the operating potential range of the acidic electrolyte.[61] Even at its open circuit potential, Sr material is immediately released into the water phase. The second cause of instability is that Ru, which is the active substance of the OER, also dissolves during the whole oxidation process (Fig. 11b). The phase transition from RuO$_2$ to RuO$_4$ occurred only at about 1.3 (vs. RHE) of Ru dissolved in acidic medium.

In order to further improve the catalytic OER durability of Ru-based perovskite oxides in acid, Na was doped at the A-site. When Na$^+$ replaces Sr^{2+}, the surface oxygen p-band center and Ru d-band center in SrRuO$_3$ are positively shifted (Fig. 11c). The binding strength between SrRuO$_3$ and the intermediate was optimized to make the activity of the OER close to the optimum. After the 20th cycle of CV, SrRuO$_3$ lost more than 85% of its initial activity, while Na$_x$Sr$_{1-x}$RuO$_3$ lost only about 15% of its initial activity in 0.1 M HClO$_4$.[62] According to DFT, Na-doping reduces the dissolution rate of Sr and Ru, resulting in higher structural stability (Fig. 11d). On the one hand, Ru is known to oxidize to the unstable Ru$^{>4+}$ at a potential above ~1.4 V (vs. RHE). The incorporation of Na$^+$ makes Ru$^{>4+}$ stable in the lattice of SrRuO$_3$, which can be used as the catalytic center to adjust its charge according to the different adsorbent. In addition, the addition of Na$^+$ reduces the deformability of RuO$_6$ octahedron, thus improving the structural stability in the OER. In general, the method of Na-doping can adjust the electron distribution state of Ru, improve the dissolution potential, and slow down the distortion of RuO$_6$ octahedron, so as to achieve
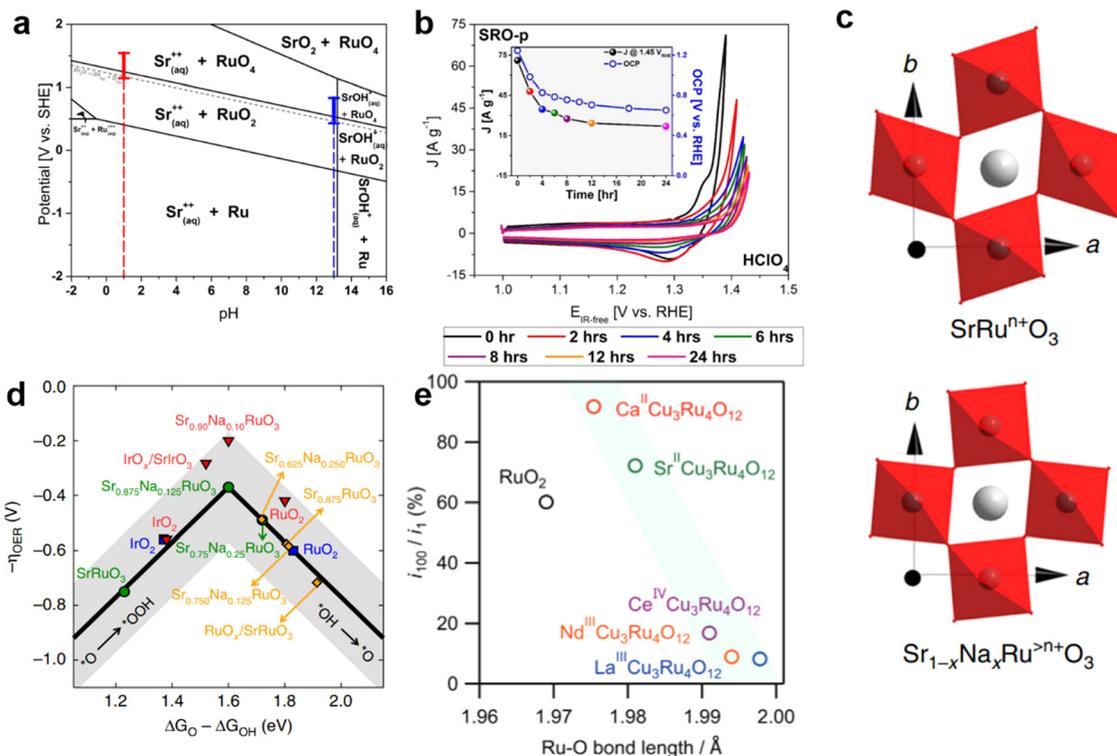
Fig. 11 (a) Pourbaix diagrams of $SrRuO_3$. (b) The CV diagram of 10 mV s^{-1} was performed at 0, 2, 4, 6, 8, 12, and 24 hours after initial contact of the $SrRuO_3$ with the synthetic air saturated electrolyte in $HClO_4$. Reproduced with permission.[61] Copyright 2017, American Chemical Society (c) Diagram of the inhibition of octahedral distortion of $SrRuO_3$ doped with Na$^+$. (d) The plot of OER Volcano-type activity. Reproduced with permission.[62] Copyright 2019, Sprinter Nature. (e) A graph showing the relationship between the length of the Ru–O bond and the ratio of current density i_{100}/i_1 at the 100th and 1st cycles. Reproduced with permission.[125] Copyright 2022, Wiley-VCH GmbH.

the purpose of enhancing the durability of Ru-based perovskite oxide in acidic media. García et al. optimized the doping of different contents of K$^+$ in $Sr_{1-x}K_xRuO_3$ (x = 0, 0.05, 0.10, 0.20) to improve the activity of the OER in O$_2$-saturated 0.1 M $HClO_4$.[63] When the current density reaches 10 mA cm^{-2}, the required voltage of $SrRuO_3$ is about 1.4 V, while the voltage of $Sr_{0.95}K_{0.05}RuO_3$ drops to about 1.35 V. After K$^+$ doping, the B-site Ru cation is oxidized to the higher oxidation state Ru^{5+}, thus alleviating the Jahn–Teller effect in the RuO_6 octahedron. The influence of cations on the distortion degree of the perovskite structure is further discussed by introducing the Goldschmidt tolerance factor (t): $t = \dfrac{\langle A-O \rangle}{\sqrt{2}\langle B-O \rangle}$. Where $\langle A–O \rangle$ and $\langle B–O \rangle$ are the main distances of ABO_3 molecular perovskite.[126] When t = 1, perovskite oxide has great symmetry. The value of t, 0.994, 0.999, 1.004 and 1.013, increases with the increase of K$^+$ content, indicating that the doping of K$^+$ could adjust the distortion degree of the perovskite structure and improve the durability.

$CaCu_3Ru_4O_{12}$ was reported to show an ultra-low overpotential of 171 mV at 10 mA cm$_{geo}^{-2}$ in 0.5 M H_2SO_4.[121] In addition, its mass activity (1942 A g$_{Ru}^{-1}$) is 170 times that of commercial RuO_2 at 1.50 V. In terms of crystal structure, the refined Ru–O bond length of $CaCu_3Ru_4O_{12}$ (1.9808(7) Å) is longer than the average Ru–O bond length of RuO2 ($\sim$1.97 Å). This indicates that the Ru–O bond strength of $CaCu_3Ru_4O_{12}$ is weaker than that of RuO_2. The theoretical OER overpotential was further

evaluated from DFT calculations. Free energy calculated on relatively stable $RuO_2(110)$ and $CaCu_3Ru_4O_{12}(001)$ surfaces. The free energy difference between ΔG_{HOO*} and ΔG_{O*} in the rate-determining step of RuO_2 is 2.08 eV, resulting in a high OER overpotential of 0.85V. For $CaCu_3Ru_4O_{12}$, $\Delta G_{HOO*}-\Delta G_{O*}$ is significantly reduced to 1.89 eV, corresponding to a theoretical overpotential of 0.66 V. This suggests that the unique quadruple structure of $CaCu_3Ru_4O_{12}$ is associated with superior activity of the OER. Shunsuke Yagi et al. further investigated the effect of A-site cations on the catalytic activity and stability of $ACu_3Ru_4O_{12}$ (A= Ca, Sr, La, Nd, Ce) in acidic aqueous solution.[125] The different cations at A-sites change the average valence states of Cu and Ru and the bond length of Ru–O. The relationship between the activity of the OER and average Cu valence shows a volcanic type relationship (Fig. 11e). In addition, it is further proved that the stability of perovskite oxide in the OER increases with the increase of Ru–O covalence with the increase of Ru–O bond length. The adjustment of different ions in quadruple perovskite oxides provides a new idea for designing OER catalysts with high activity and stability in strongly acidic aqueous solutions.

6. Conclusions and perspectives

In this review, descriptors widely accepted for the catalytic activity of perovskite oxides are first discussed. The widely
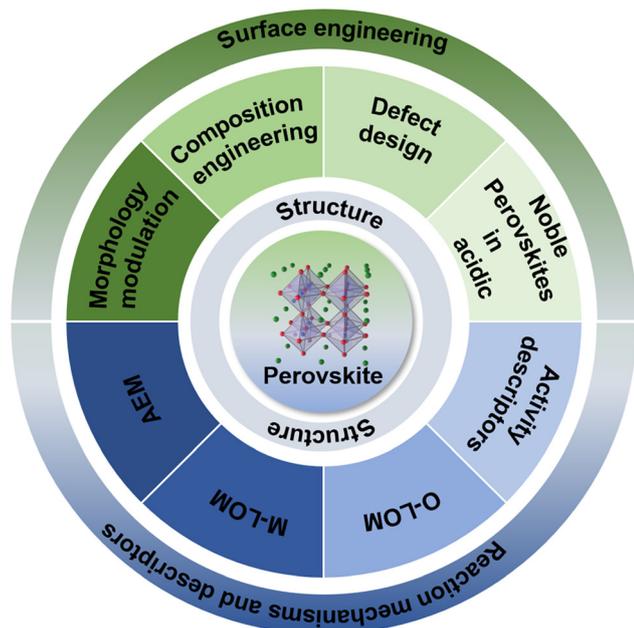
Fig. 12 A schematic representation of the strategies on the design of perovskite oxide electrocatalysts for the OER.

studied oxygen evolution mechanisms (AEM and LOM) were discussed and their differences were analyzed in terms of active sites and reaction pathways (Fig. 12). In particular, the method of regulating the mutual conversion of the AEM–LOM mechanism to obtain the best performance of the OER was introduced. On the basis of understanding these theories, the design and development of high performance OER catalysts are guided. Then, the design strategies of high efficiency perovskite oxide electrocatalysts adjusting the structure and surface in recent years, including component design, morphology control and defect engineering, were introduced. Finally, the research progress of Ir/Ru-based perovskite oxide catalysts in an acidic environment is introduced. Although perovskite oxides have made great progress in the field of the OER, there are still several directions that need further consideration in the future.

6.1. Mechanism of perovskite oxide for the OER

In the proposed oxygen evolution reaction mechanism (AEM and LOM), metals or oxygen is mainly used for the adsorption of OH and oxygen production sites. The mechanism of the OER, especially lattice oxygen, should be better understood. For example, the catalyst performance depending on the pH value is used as one of the criteria to determine the occurrence of LOM. However, the adsorption process of intermediates is poorly matched with the catalyst in the interpretation of LOM. Another, as the LOM has a lower overpotential than the AEM, has been confirmed by the DFT calculation. But its physical origin has not been explored. In particular, perovskite oxides in acidic media are often associated with dissolution and structural collapse, where the extent of LOM contribution to the OER in acidity remains to be determined. A deep understanding of the oxygen evolution mechanism of perovskite oxide is of guiding significance for the design of

high-performance catalysis, so we should further study the catalytic mechanism.

Improvements can be made in two ways. On the one hand, more efficient and accurate *in situ* characterization techniques, such as *in situ* Raman spectroscopy, *in situ* X-ray diffraction and synchrotron radiation X-ray absorption spectroscopy, are developed to realize real-time monitoring of surface changes of perovskite oxides. On the other hand, the application of complex theoretical computing techniques, machine learning and artificial intelligence can more accurately and effectively study the intermediate steps in the catalytic process, so as to guide the design of OER electrocatalysts and their further optimization. In particular, machine learning can recombine information from published experimental data and open-source databases by obtaining large amounts of material information, as opposed to high-throughput DFT approaches that rely heavily on time-consuming and expensive computational simulations.

6.2. Interface engineering of perovskite oxides

The catalytic reaction occurs on the surface of the electrocatalyst. The reactants are first adsorbed on the surface of the catalyst, then converted to products, and finally the products are desorbed from the surface of the catalyst to the electrolyte.[127] The OER reaction rate is determined by the chemical bond between the substrate molecule and the catalyst.[128] Therefore, interface engineering is very critical to the catalytic activity of perovskite oxides. On the one hand, the interface between the catalyst and electrolyte can be adjusted. Introducing foreign ions into the electrolyte to achieve dynamic equilibrium on the catalyst surface is a fast and effective way.[77,127] Alternatively, ultra-thin amorphous FeOOH nanosheets are constructed on the catalyst surface to decorate perovskite structures.[129] On the other hand, the interface is constructed in the catalyst. Integration of metals and metal compounds has received increasing attention because the Mott–Schottky effect allows the transfer of electrons between metals and metal compounds.[130] The surface of perovskite oxide can be modified to form an interface structure and achieve a strong synergistic effect.

On the whole, interfacial regulation can efficiently control the atomic and electronic structures of perovskite oxides in order to optimize chemical bond strength, electronic interaction, or achieve a synergistic impact, as well as enhance the charge transfer ability.

6.3. Practical electrolyzer test and application

Currently, most tests of OER in research are performed on rotating disk electrodes in beakers, where catalyst tests have a small area and low voltage. Laboratory testing conditions do not meet industrial requirements. Moreover, there are more uncontrollable factors in industrial application, which leads to the existing evaluation system of catalysts not being complete and accurate. For industrial applications, electrocatalysis require better performance and stability under industry-related conditions such as high current density, long working hours, high pressure and temperature.[131–133] The joint European Fuel Cell and Hydrogen Project has set a target for the industrialization of

electrolytic water, with an alkaline hydrolysis current density of 800 mA cm^{-2} and a PEM hydrolysis current density of 2500 mA cm^{-2} by 2030.[134] Therefore, the test phase in the laboratory should be carried out under simple simulation of industrial conditions (current density greater than 200 mA cm^{-2}, temperature at 50–80 °C). It is necessary to design and study more stable and efficient electrolytic water perovskite oxides.

The perovskite oxide catalyst assembled in proton exchange membrane water PEMWE for testing is also one of the keys to large-scale application. Although many transition metals have good oxygen evolution activity in acidic environments, it is tough to achieve the unity of high activity and stable structure. In order to reduce the cost, in addition to reducing the content of precious metals by utilizing the advantages of perovskite oxide structure which can accommodate a variety of elements mentioned above, it is also an effective way to maximize the catalytic efficiency of precious metals. Such as building single-atoms materials, heterogeneous structures, etc. single-atoms catalysts have been widely studied for their high catalytic efficiency. But it still faces obstacles to reuniting and shedding. So there is still a long way to go to develop perovskite oxide catalysts for practical application. In addition, PEMWE contains a number of membrane electrode components, including an electrocatalyst layer, a membrane/polymer and a porous transport layer.[135,136] The assembly of these membranes also has a great influence on the catalytic performance. It is also important to develop membrane electrode assemblies with high corrosion resistance and high-quality transmission rates. It is inferred that the industrialization of water electrolysis based on perovskite oxide electrocatalyst can be realized faster and more accurately by combining the testing and the investment of electrolytic cell under industrial conditions.

6.4. Economic considerations of perovskite oxides

Economic considerations are also important conditions for the development of perovskite oxide catalysts in the future. In order to realize the large-scale application of perovskite oxide catalysts, the technical cost should be considered. The cost, on the one hand, comes from the cost of raw materials. On the other hand, the costs are those incurred in the actual production, assembly and application processes. More economical membrane electrode components should be developed to reduce the energy consumption in the electrochemical reaction and so on.

In recent years, inorganic perovskite solar cells with excellent photoelectronic properties used as the active layer of inorganic perovskite solar cells in the field of new energy have been rapidly developed.[137–139] Decommissioned inorganic perovskite materials are rich in transition metal resources and their high value recovery is beneficial to the metal resource cycle and environmental protection. Solid wastes containing transition metals can be used as potential raw materials. Transforming them into advanced functional materials through etching and other means is more in line with the requirements of a green economy. We believe that combined efforts to develop efficient electrochemical water decomposition catalysts will accelerate

perovskite oxide catalysts to become participants in the realization of the ideal hydrogen energy society.

Conflicts of interest

There are no conflicts to declare.

Acknowledgements

References

1 R. Lee, The Outlook for Population Growth, *Science*, 2011, **333**, 569–573.

2 J. Song, C. Wei, Z.-F. Huang, C. Liu, L. Zeng, X. Wang and Z. J. Xu, A review on fundamentals for designing oxygen evolution electrocatalysts, *Chem. Soc. Rev.*, 2020, **49**, 2196–2214.

3 B. Lu, D. Wang, C. Zhao, K. Zhu, J. Yan, G. Wang, D. Cao and K. Ye, The novel dual-category active sites of NiCoP/CoP as high-performance electrocatalyst for urea electrolysis and synergistic hydrogen production, *Mater. Chem. Front.*, 2022, **6**, 1681–1689.

4 R.-Y. Fan, J.-Y. Xie, H.-J. Liu, H.-Y. Wang, M.-X. Li, N. Yu, R.-N. Luan, Y.-M. Chai and B. Dong, Directional regulating dynamic equilibrium to continuously update electrocatalytic interface for oxygen evolution reaction, *Chem. Eng. J.*, 2022, **431**, 134040.

5 T. Wang, X. Cao and L. Jiao, Ni$_2$P/NiMoP heterostructure as a bifunctional electrocatalyst for energy-saving hydrogen production, *eScience*, 2021, **1**, 69–74.

6 Y.-N. Zhou, F.-L. Wang, S.-Y. Dou, Z.-N. Shi, B. Dong, W.-L. Yu, H.-Y. Zhao, F.-G. Wang, J.-F. Yu and Y.-M. Chai, Motivating high-valence Nb doping by fast molten salt method for NiFe hydroxides toward efficient oxygen evolution reaction, *Chem. Eng. J.*, 2022, **427**, 131643.

7 X. Li, Q. Hu, H. Yang, T. Ma, X. Chai and C. He, Bimetallic two-dimensional materials for electrocatalytic oxygen evolution, *Chin. Chem. Lett.*, 2022, **33**, 3657–3671.

8 J.-I. Jung, H. Y. Jeong, M. G. Kim, G. Nam, J. Park and J. Cho, Fabrication of Ba$_{0.5}$Sr$_{0.5}$Co$_{0.8}$Fe$_{0.2}$O$_{3-\delta}$ Catalysts with Enhanced Electrochemical Performance by Removing an Inherent Heterogeneous Surface Film Layer, *Adv. Mater.*, 2015, **27**, 266–271.

9 Z. Song, X. Wang, F. Liu, Q. Zhou, W.-J. Yin, H. Wu, W. Deng and J. Wang, Distilling universal activity descriptors for perovskite catalysts from multiple data sources via multi-task symbolic regression, *Mater. Horiz.*, 2023, **10**, 1651–1660.

10 Y. Bu, S. Kim, O. Kwon, Q. Zhong and G. Kim, A Composite Catalyst Based on Perovskites for Overall Water Splitting in Alkaline Conditions, *ChemElectroChem*, 2019, **6**, 1520–1524.

11 J. Chen, J. Wu, Y. Liu, X. Hu and D. Geng, Assemblage of Perovskite LaNiO₃ Connected With In Situ Grown Nitrogen-Doped Carbon Nanotubes as High-Performance Electrocatalyst for Oxygen Evolution Reaction, *Phys. Status Solidi A*, 2018, **215**, 1800380.

12 O. Diaz-Morales, S. Raaijman, R. Kortlever, P. J. Kooyman, T. Wezendonk, J. Gascon, W. T. Fu and M. T. M. Koper, Iridium-based double perovskites for efficient water oxidation in acid media, *Nat. Commun.*, 2016, **7**, 12363.

13 X. Xu, Y. Zhong and Z. Shao, Double Perovskites in Catalysis, Electrocatalysis, and Photo(electro)catalysis, *Trends Chem.*, 2019, **1**, 410–424.

14 N.-I. Kim, Y. J. Sa, T. S. Yoo, S. R. Choi, R. A. Afzal, T. Choi, Y.-S. Seo, K.-S. Lee, J. Y. Hwang, W. S. Choi, S. H. Joo and J.-Y. Park, Oxygen-deficient triple perovskites as highly active and durable bifunctional electrocatalysts for oxygen electrode reactions, *Sci. Adv.*, 2018, **4**, eaap9360.

15 I. Yamada, H. Fujii, A. Takamatsu, H. Ikeno, K. Wada, H. Tsukasaki, S. Kawaguchi, S. Mori and S. Yagi, Bifunctional Oxygen Reaction Catalysis of Quadruple Manganese Perovskites, *Adv. Mater.*, 2017, **29**, 1603004.

16 X. Xu, Y. Pan, Y. Zhong, R. Ran and Z. Shao, Ruddlesden–Popper perovskites in electrocatalysis, *Mater. Horiz.*, 2020, **7**, 2519–2565.

17 J. Hwang, R. R. Rao, L. Giordano, Y. Katayama, Y. Yu and Y. Shao-Horn, Perovskites in catalysis and electrocatalysis, *Science*, 2017, **358**, 751–756.

18 S. Hao, M. Liu, J. Pan, X. Liu, X. Tan, N. Xu, Y. He, L. Lei and X. Zhang, Dopants fixation of Ruthenium for boosting acidic oxygen evolution stability and activity, *Nat. Commun.*, 2020, **11**, 5368.

19 C. R. Lhermitte and B. M. Bartlett, Advancing the Chemistry of CuWO₄ for Photoelectrochemical Water Oxidation, *Acc. Chem. Res.*, 2016, **49**, 1121–1129.

20 T. Liu, Q. Zhang and Q. Zhao, Theoretical insight into the anion vacancy healing process during the oxygen evolution reaction on TaON and Ta₃N₅, *Phys. Chem. Chem. Phys.*, 2022, **24**, 13999–14006.

21 V. F. Mattick, X. Jin, T. Yang, R. E. White and K. Huang, Unraveling Oxygen Electrocatalysis Mechanisms on a Thin-Film Oxygen-Deficient Perovskite La₀.₆Sr₀.₄CoO₃₋δ, *ACS Appl. Energy Mater.*, 2018, **1**, 3937–3946.

22 Y. Sun, R. Li, X. Chen, J. Wu, Y. Xie, X. Wang, K. Ma, L. Wang, Z. Zhang, Q. Liao, Z. Kang and Y. Zhang, A-Site Management Prompts the Dynamic Reconstructed Active Phase of Perovskite Oxide OER Catalysts, *Adv. Energy Mater.*, 2021, **11**, 2003755.

23 L. Zhao, K. Chen, Y. Liu and B. He, A novel layered perovskite as symmetric electrode for direct hydrocarbon solid oxide fuel cells, *J. Power Sources*, 2017, **342**, 313–319.

24 V. Tripkovic, H. A. Hansen, J. M. Garcia-Lastra and T. Vegge, Comparative DFT+U and HSE Study of the Oxygen Evolution Electrocatalysis on Perovskite Oxides, *J. Phys. Chem. C*, 2018, **122**, 1135–1147.

25 S. Lee, M. R. Ashwin Kishore, D. Kim, H. Kang, J. Chun, L. S. Oh, J. H. Park, H. J. Kim, J. S. Yoo and E. Lim, Direct O–O Coupling Promoted the Oxygen Evolution Reaction by Dual Active Sites from Ag/LaNiO₃ Interfaces, *ACS Appl. Energy Mater.*, 2022, **5**, 14658–14668.

26 M. T. M. Koper, Theory of multiple proton–electron transfer reactions and its implications for electrocatalysis, *Chem. Sci.*, 2013, **4**, 2710–2723.

27 S. Vasala and M. Karppinen, A₂B′B″O₆ perovskites: A review, *Prog. Solid State Chem.*, 2015, **43**, 1–36.

28 Z. Wang, Z. Hao, F. Shi, K. Zhu, X. Zhu and W. Yang, Boosting the oxygen evolution reaction through migrating active sites from the bulk to surface of perovskite oxides, *J. Energy Chem.*, 2022, **69**, 434–441.

29 I. C. Man, H.-Y. Su, F. Calle-Vallejo, H. A. Hansen, J. I. Martínez, N. G. Inoglu, J. Kitchin, T. F. Jaramillo, J. K. Nørskov and J. Rossmeisl, Universality in Oxygen Evolution Electrocatalysis on Oxide Surfaces, *ChemCatChem*, 2011, **3**, 1159–1165.

30 J. O. M. Bockris and T. Otagawa, The Electrocatalysis of Oxygen Evolution on Perovskites, *J. Electrochem. Soc.*, 1984, **131**, 290.

31 Y. Matsumoto and E. Sato, Electrocatalytic properties of transition metal oxides for oxygen evolution reaction, *Mater. Chem. Phys.*, 1986, **14**, 397–426.

32 A. Grimaud, O. Diaz-Morales, B. Han, W. T. Hong, Y.-L. Lee, L. Giordano, K. A. Stoerzinger, M. T. M. Koper and Y. Shao-Horn, Activating lattice oxygen redox reactions in metal oxides to catalyse oxygen evolution, *Nat. Chem.*, 2017, **9**, 457–465.

33 A. Grimaud, A. Demortière, M. Saubanère, W. Dachraoui, M. Duchamp, M.-L. Doublet and J.-M. Tarascon, Activation of surface oxygen sites on an iridium-based model catalyst for the oxygen evolution reaction, *Nat. Energy*, 2016, **2**, 16189.

34 J. T. Mefford, X. Rong, A. M. Abakumov, W. G. Hardin, S. Dai, A. M. Kolpak, K. P. Johnston and K. J. Stevenson, Water electrolysis on La₁₋ₓSrₓCoO₃₋δ perovskite electrocatalysts, *Nat. Commun.*, 2016, **7**, 11053.

35 Y. Pan, X. Xu, Y. Zhong, L. Ge, Y. Chen, J.-P. M. Veder, D. Guan, R. O'Hayre, M. Li, G. Wang, H. Wang, W. Zhou and Z. Shao, Direct evidence of boosted oxygen evolution over perovskite by enhanced lattice oxygen participation, *Nat. Commun.*, 2020, **11**, 2002.

36 X. Rong, J. Parolin and A. M. Kolpak, A Fundamental Relationship between Reaction Mechanism and Stability in Metal Oxide Catalysts for Oxygen Evolution, *ACS Catal.*, 2016, **6**, 1153–1158.

37 J.-W. Zhao, H. Zhang, C.-F. Li, X. Zhou, J.-Q. Wu, F. Zeng, J. Zhang and G.-R. Li, Key roles of surface Fe sites and Sr vacancies in the perovskite for an efficient oxygen evolution reaction via lattice oxygen oxidation, *Energy Environ. Sci.*, 2022, **15**, 3912–3922.

38 M. Lu, Y. Zheng, Y. Hu, B. Huang, D. Ji, M. Sun, J. Li, Y. Peng, R. Si, P. Xi and C.-H. Yan, Artificially steering electrocatalytic oxygen evolution reaction mechanism by regulating oxygen defect contents in perovskites, *Sci. Adv.*, 2022, **8**, eabq3563.

39 J. Suntivich, K. J. May, H. A. Gasteiger, J. B. Goodenough and Y. Shao-Horn, A Perovskite Oxide Optimized for Oxygen Evolution Catalysis from Molecular Orbital Principles, *Science*, 2011, **334**, 1383–1385.

40 Z.-F. Huang, J. Song, Y. Du, S. Xi, S. Dou, J. M. V. Nsanzimana, C. Wang, Z. J. Xu and X. Wang, Chemical and structural origin of lattice oxygen oxidation in Co–Zn oxyhydroxide oxygen evolution electrocatalysts, *Nat. Energy*, 2019, **4**, 329–338.

41 T. Wu, S. Sun, J. Song, S. Xi, Y. Du, B. Chen, W. A. Sasangka, H. Liao, C. L. Gan, G. G. Scherer, L. Zeng, H. Wang, H. Li, A. Grimaud and Z. J. Xu, Iron-facilitated dynamic active-site generation on spinel $CoAl_2O_4$ with self-termination of surface reconstruction for water oxidation, *Nat. Catal.*, 2019, **2**, 763–772.

42 Y. Duan, S. Sun, Y. Sun, S. Xi, X. Chi, Q. Zhang, X. Ren, J. Wang, S. J. H. Ong, Y. Du, L. Gu, A. Grimaud and Z. J. Xu, Mastering Surface Reconstruction of Metastable Spinel Oxides for Better Water Oxidation, *Adv. Mater.*, 2019, **31**, 1807898.

43 J. Zaanen, G. A. Sawatzky and J. W. Allen, Band gaps and electronic structure of transition-metal compounds, *Phys. Rev. Lett.*, 1985, **55**, 418–421.

44 A. K. Tomar, U. N. Pan, N. H. Kim and J. H. Lee, Enabling Lattice Oxygen Participation in a Triple Perovskite Oxide Electrocatalyst for the Oxygen Evolution Reaction, *ACS Energy Lett.*, 2023, **8**, 565–573.

45 H. Chen, C. Lim, M. Zhou, Z. He, X. Sun, X. Li, Y. Ye, T. Tan, H. Zhang, C. Yang, J. W. Han and Y. Chen, Activating Lattice Oxygen in Perovskite Oxide by B-Site Cation Doping for Modulated Stability and Activity at Elevated Temperatures, *Adv. Sci.*, 2021, **8**, 2102713.

46 G. T. K. K. Gunasooriya and J. K. Nørskov, Analysis of Acid-Stable and Active Oxides for the Oxygen Evolution Reaction, *ACS Energy Lett.*, 2020, **5**, 3778–3787.

47 Z. Shi, X. Wang, J. Ge, C. Liu and W. Xing, Fundamental understanding of the acidic oxygen evolution reaction: mechanism study and state-of-the-art catalysts, *Nanoscale*, 2020, **12**, 13249–13275.

48 J. Zhu, S. Li, Z. Zhuang, S. Gao, X. Hong, X. Pan, R. Yu, L. Zhou, L. V. Moskaleva and L. Mai, Ultrathin Metal Silicate Hydroxide Nanosheets with Moderate Metal–Oxygen Covalency Enables Efficient Oxygen Evolution, *Energy Environ. Mater.*, 2022, **5**, 231–237.

49 L. Heymann, M. L. Weber, M. Wohlgemuth, M. Risch, R. Dittmann, C. Baeumer and F. Gunkel, Separating the Effects of Band Bending and Covalency in Hybrid Perovskite Oxide Electrocatalyst Bilayers for Water Electrolysis, *ACS Appl. Mater. Interfaces*, 2022, **14**, 14129–14136.

50 Z.-Y. Yu, Y. Duan, Y. Kong, X.-L. Zhang, X.-Y. Feng, Y. Chen, H. Wang, X. Yu, T. Ma, X. Zheng, J. Zhu, M.-R. Gao and S.-H. Yu, General Synthesis of Tube-like Nano-structured Perovskite Oxides with Tunable Transition Metal–Oxygen Covalency for Efficient Water Electrooxidation in Neutral Media, *J. Am. Chem. Soc.*, 2022, **144**, 13163–13173.

51 Z. Shen, M. Qu, J. Shi, F. E. Oropeza, V. A. de la Peña O'Shea, G. Gorni, C. M. Tian, J. P. Hofmann, J. Cheng, J. Li and K. H. L. Zhang, Correlating the electronic structure of perovskite $La_{1-x}Sr_xCoO_3$ with activity for the oxygen

evolution reaction: The critical role of Co 3d hole state, *J. Energy Chem.*, 2022, **65**, 637–645.

52 H. Wang, J. Wang, Y. Pi, Q. Shao, Y. Tan and X. Huang, Double Perovskite $LaFe_xNi_{1-x}O_3$ Nanorods Enable Efficient Oxygen Evolution Electrocatalysis, *Angew. Chem., Int. Ed.*, 2019, **58**, 2316–2320.

53 Y. Tong, J. Wu, P. Chen, H. Liu, W. Chu, C. Wu and Y. Xie, Vibronic Superexchange in Double Perovskite Electrocatalyst for Efficient Electrocatalytic Oxygen Evolution, *J. Am. Chem. Soc.*, 2018, **140**, 11165–11169.

54 A. L. Hoang, S. Balakrishnan, A. Hodges, G. Tsekouras, A. Al-Musawi, K. Wagner, C.-Y. Lee, G. F. Swiegers and G. G. Wallace, High-performing catalysts for energy-efficient commercial alkaline water electrolysis, *Sustainable Energy Fuels*, 2023, **7**, 31–60.

55 J. Qian, T. Wang, Z. Zhang, Y. Liu, J. Li and D. Gao, Engineered spin state in Ce doped $LaCoO_3$ with enhanced electrocatalytic activity for rechargeable Zn–Air batteries, *Nano Energy*, 2020, **74**, 104948.

56 D. A. Kumar, S. Selvasekarapandian, H. Nithya, J. Leiro, Y. Masuda, S.-D. Kim and S.-K. Woo, Effect of calcium doping on $LaCoO_3$ prepared by Pechini method, *Powder Technol.*, 2013, **235**, 140–147.

57 J. Qian, J. Li, B. Xia, J. Zhang, Z. Zhang, C. Guan, D. Gao and W. Huang, Multi-stability modulating of alkaline-earth metal doped $LaCoO_3$ for rechargeable Zn–air batteries, *Energy Storage Mater.*, 2021, **42**, 470–476.

58 L. He, Y. Zhang, Y. Zang, C. Liu, W. Wang, R. Han, N. Ji, S. Zhang and Q. Liu, Promotion of A-Site Ag-Doped Perovskites for the Catalytic Oxidation of Soot: Synergistic Catalytic Effect of Dual Active Sites, *ACS Catal.*, 2021, **11**, 14224–14236.

59 C. Liu, D. Ji, H. Shi, Z. Wu, H. Huang, Z. Kang and Z. Chen, An A-site management and oxygen-deficient regulation strategy with a perovskite oxide electrocatalyst for the oxygen evolution reaction, *J. Mater. Chem. A*, 2022, **10**, 1336–1342.

60 S. H. Chang, N. Danilovic, K.-C. Chang, R. Subbaraman, A. P. Paulikas, D. D. Fong, M. J. Highland, P. M. Baldo, V. R. Stamenkovic, J. W. Freeland, J. A. Eastman and N. M. Markovic, Functional links between stability and reactivity of strontium ruthenate single crystals during oxygen evolution, *Nat. Commun.*, 2014, **5**, 4191.

61 B.-J. Kim, D. F. Abbott, X. Cheng, E. Fabbri, M. Nachtegaal, F. Bozza, I. E. Castelli, D. Lebedev, R. Schäublin, C. Copéret, T. Graule, N. Marzari and T. J. Schmidt, Unraveling Thermodynamics, Stability, and Oxygen Evolution Activity of Strontium Ruthenium Perovskite Oxide, *ACS Catal.*, 2017, **7**, 3245–3256.

62 M. Retuerto, L. Pascual, F. Calle-Vallejo, P. Ferrer, D. Gianolio, A. G. Pereira, Á. García, J. Torrero, M. T. Fernández-Díaz, P. Bencok, M. A. Peña, J. L. G. Fierro and S. Rojas, Na-doped ruthenium perovskite electrocatalysts with improved oxygen evolution activity and durability in acidic media, *Nat. Commun.*, 2019, **10**, 2041.

63 I. Rodríguez-García, D. Galyamin, L. Pascual, P. Ferrer, M. A. Peña, D. Grinter, G. Held, M. Abdel Salam,

M. Mokhtar, K. Narasimharao, M. Retuerto and S. Rojas, Enhanced stability of SrRuO$_3$ mixed oxide via monovalent doping in Sr$_{1-x}$K$_x$RuO$_3$ for the oxygen evolution reaction, *J. Power Sources*, 2022, **521**, 230950.

64 H.-T. Jeng, S.-H. Lin and C.-S. Hsue, Orbital Ordering and Jahn–Teller Distortion in Perovskite Ruthenate SrRuO$_3$, *Phys. Rev. Lett.*, 2006, **97**, 067002.

65 Y. Zhu, W. Zhou, J. Yu, Y. Chen, M. Liu and Z. Shao, Enhancing Electrocatalytic Activity of Perovskite Oxides by Tuning Cation Deficiency for Oxygen Reduction and Evolution Reactions, *Chem. Mater.*, 2016, **28**, 1691–1697.

66 H. Jo, Y. Yang, A. Seong, D. Jeong, J. Kim, S. H. Joo, Y. J. Kim, L. Zhang, Z. Liu, J.-Q. Wang, S. K. Kwak and G. Kim, Promotion of the oxygen evolution reaction via the reconstructed active phase of perovskite oxide, *J. Mater. Chem. A*, 2022, **10**, 2271–2279.

67 G. Chen, Z. Hu, Y. Zhu, Z.-G. Chen, Y. Zhong, H.-J. Lin, C.-T. Chen, L. H. Tjeng, W. Zhou and Z. Shao, Ultrahigh-performance tungsten-doped perovskites for the oxygen evolution reaction, *J. Mater. Chem. A*, 2018, **6**, 9854–9859.

68 J. Xiong, H. Zhong, J. Li, X. Zhang, J. Shi, W. Cai, K. Qu, C. Zhu, Z. Yang, S. P. Beckman and H. Cheng, Engineering highly active oxygen sites in perovskite oxides for stable and efficient oxygen evolution, *Appl. Catal., B*, 2019, **256**, 117817.

69 J. Ran, T. Wang, J. Zhang, Y. Liu, C. Xu, S. Xi and D. Gao, Modulation of Electronics of Oxide Perovskites by Sulfur Doping for Electrocatalysis in Rechargeable Zn–Air Batteries, *Chem. Mater.*, 2020, **32**, 3439–3446.

70 Y. Zhu, Q. Lin, Z. Wang, D. Qi, Y. Yin, Y. Liu, X. Zhang, Z. Shao and H. Wang, Chlorine-anion doping induced multi-factor optimization in perovskties for boosting intrinsic oxygen evolution, *J. Energy Chem.*, 2021, **52**, 115–120.

71 L. Tang, Y. Yang, H. Guo, Y. Wang, M. Wang, Z. Liu, G. Yang, X. Fu, Y. Luo, C. Jiang, Y. Zhao, Z. Shao and Y. Sun, High Configuration Entropy Activated Lattice Oxygen for O$_2$ Formation on Perovskite Electrocatalyst, *Adv. Funct. Mater.*, 2022, **32**, 2112157.

72 T. X. Nguyen, Y.-C. Liao, C.-C. Lin, Y.-H. Su and J.-M. Ting, Advanced High Entropy Perovskite Oxide Electrocatalyst for Oxygen Evolution Reaction, *Adv. Funct. Mater.*, 2021, **31**, 2101632.

73 G. Valderrama, A. Kiennemann, C. U. de Navarro and M. R. Goldwasser, LaNi$_{1-x}$Mn$_x$O$_3$ perovskite-type oxides as catalysts precursors for dry reforming of methane, *Appl. Catal., A*, 2018, **565**, 26–33.

74 X. Shen, Y. Sun, Y. Wu, J. Wang, E. Jiang, X. Xu, J. Su and Z. Jia, The coupling of CH$_4$ partial oxidation and CO$_2$ splitting for syngas production via double perovskite-type oxides LaFe$_x$Co$_{1-x}$O$_3$, *Fuel*, 2020, **268**, 117381.

75 X. Cheng, B.-J. Kim, E. Fabbri and T. J. Schmidt, Co/Fe Oxyhydroxides Supported on Perovskite Oxides as Oxygen Evolution Reaction Catalyst Systems, *ACS Appl. Mater. Interfaces*, 2019, **11**, 34787–34795.

76 B. W. Kwon, J. H. Oh, G. S. Kim, S. P. Yoon, J. Han, S. W. Nam and H. C. Ham, The novel perovskite-type Ni-doped

Sr$_{0.92}$Y$_{0.08}$TiO$_3$ catalyst as a reforming biogas (CH$_4$ + CO$_2$) for H$_2$ production, *Appl. Energy*, 2018, **227**, 213–219.

77 N. Yu, H.-J. Liu, Y.-N. Cao, Q.-Y. Wang, Y. Ma, J.-F. Yu, H. Hu, Y.-M. Chai and B. Dong, Dynamic equilibrium of external Fe^{3+} to effectively construct catalytic surface of perovskite LaNi$_{1-x}$Fe$_x$O$_3$ for water oxidation, *Colloids Surf., A*, 2022, **654**, 130042.

78 N. Yu, X.-Y. Zhang, Q.-Y. Wang, H.-J. Liu, G. Han, F.-G. Wang, Y.-L. Zhou, Y.-M. Chai and B. Dong, Electrochemical activation construction of LaCo$_{1-x-y}$Ni$_x$Fe$_y$O$_3$ promoted by optimized lattice Ni doping toward water oxidation, *Int. J. Hydrogen Energy*, 2022, **47**, 39097–39107.

79 B.-J. Kim, E. Fabbri, D. F. Abbott, X. Cheng, A. H. Clark, M. Nachtegaal, M. Borlaf, I. E. Castelli, T. Graule and T. J. Schmidt, Functional Role of Fe-Doping in Co-Based Perovskite Oxide Catalysts for Oxygen Evolution Reaction, *J. Am. Chem. Soc.*, 2019, **141**, 5231–5240.

80 A. Grimaud, K. J. May, C. E. Carlton, Y.-L. Lee, M. Risch, W. T. Hong, J. Zhou and Y. Shao-Horn, Double perovskites as a family of highly active catalysts for oxygen evolution in alkaline solution, *Nat. Commun.*, 2013, **4**, 2439.

81 Y. Zhu, W. Zhou, J. Sunarso, Y. Zhong and Z. Shao, Phosphorus-Doped Perovskite Oxide as Highly Efficient Water Oxidation Electrocatalyst in Alkaline Solution, *Adv. Funct. Mater.*, 2016, **26**, 5862–5872.

82 K. I. Kobayashi, T. Kimura, H. Sawada, K. Terakura and Y. Tokura, Room-temperature magnetoresistance in an oxide material with an ordered double-perovskite structure, *Nature*, 1998, **395**, 677–680.

83 M. García-Hernández, J. L. Martínez, M. J. Martínez-Lope, M. T. Casais and J. A. Alonso, Finding Universal Correlations between Cationic Disorder and Low Field Magnetoresistance in FeMo Double Perovskite Series, *Phys. Rev. Lett.*, 2001, **86**, 2443–2446.

84 S. Zhao, L. Shi, S. Zhou, J. Zhao, H. Yang and Y. Guo, Size-dependent magnetic properties and Raman spectra of La$_2$NiMnO$_6$ nanoparticles, *J. Appl. Phys.*, 2009, **106**, 123901.

85 J. F. Shin, A. Orera, D. C. Apperley and P. R. Slater, Oxyanion doping strategies to enhance the ionic conductivity in Ba$_2$In$_2$O$_5$, *J. Mater. Chem.*, 2011, **21**, 874–879.

86 J. M. Porras-Vazquez, T. F. Kemp, J. V. Hanna and P. R. Slater, Synthesis and characterisation of oxyanion-doped manganites for potential application as SOFC cathodes, *J. Mater. Chem.*, 2012, **22**, 8287–8293.

87 J. M. Porras-Vazquez, T. Pike, C. A. Hancock, J. F. Marco, F. J. Berry and P. R. Slater, Investigation into the effect of Si doping on the performance of SrFeO$_{3-\delta}$ SOFC electrode materials, *J. Mater. Chem. A*, 2013, **1**, 11834–11841.

88 H. Wang, Y.-F. Yu, Q.-W. Chen and K. Cheng, Carboxyl-functionalized nanoparticles with magnetic core and mesopore carbon shell as adsorbents for the removal of heavy metal ions from aqueous solution, *Dalton Trans.*, 2011, **40**, 559–563.

89 J. Li, S. Bernard, V. Salles, C. Gervais and P. Miele, Preparation of Polyborazylene-Derived Bulk Boron Nitride with Tunable Properties by Warm-Pressing and Pressureless Pyrolysis, *Chem. Mater.*, 2010, **22**, 2010–2019.

90 B. Hua, M. Li, W. Pang, W. Tang, S. Zhao, Z. Jin, Y. Zeng, B. Shalchi Amirkhiz and J.-L. Luo, Activating p-Blocking Centers in Perovskite for Efficient Water Splitting, *Chem*, 2018, **4**, 2902–2916.

91 Y. Zhu, W. Zhou, Y. Zhong, Y. Bu, X. Chen, Q. Zhong, M. Liu and Z. Shao, A Perovskite Nanorod as Bifunctional Electrocatalyst for Overall Water Splitting, *Adv. Energy Mater.*, 2017, **7**, 1602122.

92 S. Bie, Y. Zhu, J. Su, C. Jin, S. Liu, R. Yang and J. Wu, One-pot fabrication of yolk–shell structured $La_{0.9}Sr_{0.1}CoO_3$ perovskite microspheres with enhanced catalytic activities for oxygen reduction and evolution reactions, *J. Mater. Chem. A*, 2015, **3**, 22448–22453.

93 J. Kim, X. Chen, P.-C. Shih and H. Yang, Porous Perovskite-Type Lanthanum Cobaltite as Electrocatalysts toward Oxygen Evolution Reaction, *ACS Sustainable Chem. Eng.*, 2017, **5**, 10910–10917.

94 J. Dai, Y. Zhu, Y. Zhong, J. Miao, B. Lin, W. Zhou and Z. Shao, Enabling High and Stable Electrocatalytic Activity of Iron-Based Perovskite Oxides for Water Splitting by Combined Bulk Doping and Morphology Designing, *Adv. Mater. Interfaces*, 2019, **6**, 1801317.

95 S. Zhou, X. Miao, X. Zhao, C. Ma, Y. Qiu, Z. Hu, J. Zhao, L. Shi and J. Zeng, Engineering electrocatalytic activity in nanosized perovskite cobaltite through surface spin-state transition, *Nat. Commun.*, 2016, **7**, 11510.

96 C. Jin, X. Cao, L. Zhang, C. Zhang and R. Yang, Preparation and electrochemical properties of urchin-like $La_{0.8}Sr_{0.2}MnO_3$ perovskite oxide as a bifunctional catalyst for oxygen reduction and oxygen evolution reaction, *J. Power Sources*, 2013, **241**, 225–230.

97 H.-Y. Wang, S.-F. Hung, H.-Y. Chen, T.-S. Chan, H. M. Chen and B. Liu, In Operando Identification of Geometrical-Site-Dependent Water Oxidation Activity of Spinel Co_3O_4, *J. Am. Chem. Soc.*, 2016, **138**, 36–39.

98 S. Malkhandi, P. Trinh, A. K. Manohar, A. Manivannan, M. Balasubramanian, G. K. S. Prakash and S. R. Narayanan, Design Insights for Tuning the Electrocatalytic Activity of Perovskite Oxides for the Oxygen Evolution Reaction, *J. Phys. Chem. C*, 2015, **119**, 8004–8013.

99 H. A. Tahini, X. Tan, U. Schwingenschlögl and S. C. Smith, Formation and Migration of Oxygen Vacancies in $SrCoO_3$ and Their Effect on Oxygen Evolution Reactions, *ACS Catal.*, 2016, **6**, 5565–5570.

100 E. Marelli, J. Gazquez, E. Poghosyan, E. Müller, D. J. Gawryluk, E. Pomjakushina, D. Sheptyakov, C. Piamonteze, D. Aegerter, T. J. Schmidt, M. Medarde and E. Fabbri, Correlation between Oxygen Vacancies and Oxygen Evolution Reaction Activity for a Model Electrode: $PrBaCo_2O_{5+\delta}$, *Angew. Chem., Int. Ed.*, 2021, **60**, 14609–14619.

101 J. Kim, X. Yin, K.-C. Tsao, S. Fang and H. Yang, $Ca_2Mn_2O_5$ as Oxygen-Deficient Perovskite Electrocatalyst for Oxygen Evolution Reaction, *J. Am. Chem. Soc.*, 2014, **136**, 14646–14649.

102 Y. Lu, A. Ma, Y. Yu, R. Tan, C. Liu, P. Zhang, D. Liu and J. Gui, Engineering Oxygen Vacancies into $LaCoO_3$ Perovskite for Efficient Electrocatalytic Oxygen Evolution, *ACS Sustainable Chem. Eng.*, 2019, **7**, 2906–2910.

103 J. Bian, Z. Li, N. Li and C. Sun, Oxygen Deficient $LaMn_{0.75}Co_{0.25}O_{3-\delta}$ Nanofibers as an Efficient Electrocatalyst for Oxygen Evolution Reaction and Zinc–Air Batteries, *Inorg. Chem.*, 2019, **58**, 8208–8214.

104 L. Wang, K. A. Stoerzinger, L. Chang, X. Yin, Y. Li, C. S. Tang, E. Jia, M. E. Bowden, Z. Yang, A. Abdelsamie, L. You, R. Guo, J. Chen, A. Rusydi, J. Wang, S. A. Chambers and Y. Du, Strain Effect on Oxygen Evolution Reaction Activity of Epitaxial $NdNiO_3$ Thin Films, *ACS Appl. Mater. Interfaces*, 2019, **11**, 12941–12947.

105 J. R. Petrie, H. Jeen, S. C. Barron, T. L. Meyer and H. N. Lee, Enhancing Perovskite Electrocatalysis through Strain Tuning of the Oxygen Deficiency, *J. Am. Chem. Soc.*, 2016, **138**, 7252–7255.

106 H. Wang, J. Qi, N. Yang, W. Cui, J. Wang, Q. Li, Q. Zhang, X. Yu, L. Gu, J. Li, R. Yu, K. Huang, S. Song, S. Feng and D. Wang, Dual-Defects Adjusted Crystal-Field Splitting of $LaCo_{1-x}Ni_xO_{3-\delta}$ Hollow Multishelled Structures for Efficient Oxygen Evolution, *Angew. Chem., Int. Ed.*, 2020, **59**, 19691–19695.

107 F. You, J. Wan, J. Qi, D. Mao, N. Yang, Q. Zhang, L. Gu and D. Wang, Lattice Distortion in Hollow Multi-Shelled Structures for Efficient Visible-Light CO2 Reduction with a SnS_2/SnO_2 Junction, *Angew. Chem., Int. Ed.*, 2020, **59**, 721–724.

108 D. N. Mueller, M. L. Machala, H. Bluhm and W. C. Chueh, Redox activity of surface oxygen anions in oxygen-deficient perovskite oxides during electrochemical reactions, *Nat. Commun.*, 2015, **6**, 6097.

109 L. Yan, Y. Lin, X. Yu, W. Xu, T. Salas, H. Smallidge, M. Zhou and H. Luo, $La_{0.8}Sr_{0.2}MnO_3$-Based Perovskite Nanoparticles with the A-Site Deficiency as High Performance Bifunctional Oxygen Catalyst in Alkaline Solution, *ACS Appl. Mater. Interfaces*, 2017, **9**, 23820–23827.

110 Y. Xue, H. Miao, S. Sun, Q. Wang, S. Li and Z. Liu, $(La_{1-x}Sr_x)_{0.98}MnO_3$ perovskite with A-site deficiencies toward oxygen reduction reaction in aluminum-air batteries, *J. Power Sources*, 2017, **342**, 192–201.

111 L. Tang, Y. Rao, L. Wei, H. Zheng, H. Liu, W. Zhang and K. Tang, A-site Cation Defects $(Ba_{0.5}Sr_{0.5})_{1-x}Co_{0.8}Fe_{0.2}O_{3-\delta}$ Perovskites as Active Oxygen Evolution Reaction Catalyst in Alkaline Electrolyte†, *Chin. J. Chem.*, 2021, **39**, 2692–2698.

112 N. Li, J. Guo, Y. Ding, Y. Hu, C. Zhao and C. Zhao, Direct Regulation of Double Cation Defects at the A1A2 Site for a High-Performance Oxygen Evolution Reaction Perovskite Catalyst, *ACS Appl. Mater. Interfaces*, 2021, **13**, 332–340.

113 Y. Shi, K. Huang, L. Shen, C. Ding, Z. Lu, H. Tan, C. Guo and C. Yan, Understanding the in-plane electron transport in low noble metal proton exchange membrane water electrolyser, *J. Power Sources*, 2022, **549**, 232130.

114 M. Upadhyay, A. Kim, S. S. Paramanantham, H. Kim, D. Lim, S. Lee, S. Moon and H. Lim, Three-dimensional CFD simulation of proton exchange membrane water electrolyser: Performance assessment under different condition, *Appl. Energy*, 2022, **306**, 118016.

115 F. Barbir, PEM electrolysis for production of hydrogen from renewable energy sources, *Sol. Energy*, 2005, **78**, 661–669.

116 L. C. Seitz, C. F. Dickens, K. Nishio, Y. Hikita, J. Montoya, A. Doyle, C. Kirk, A. Vojvodic, H. Y. Hwang, J. K. Norskov and T. F. Jaramillo, A highly active and stable IrO_x $SrIrO_3$ catalyst for the oxygen evolution reaction, *Science*, 2016, **353**, 1011–1014.

117 L. Yang, G. Yu, X. Ai, W. Yan, H. Duan, W. Chen, X. Li, T. Wang, C. Zhang, X. Huang, J.-S. Chen and X. Zou, Efficient oxygen evolution electrocatalysis in acid by a perovskite with face-sharing IrO_6 octahedral dimers, *Nat. Commun.*, 2018, **9**, 5236.

118 N. Li, L. Cai, C. Wang, Y. Lin, J. Huang, H. Sheng, H. Pan, W. Zhang, Q. Ji, H. Duan, W. Hu, W. Zhang, F. Hu, H. Tan, Z. Sun, B. Song, S. Jin and W. Yan, Identification of the Active-Layer Structures for Acidic Oxygen Evolution from $9R-BaIrO_3$ Electrocatalyst with Enhanced Iridium Mass Activity, *J. Am. Chem. Soc.*, 2021, **143**, 18001–18009.

119 R. Zhang, N. Dubouis, M. B. Osman, W. Yin, M. T. Sougrati, D. A. D. Corte, D. Giaume and A. Grimaud, A Dissolution/Precipitation Equilibrium on the Surface of Iridium-Based Perovskites Controls Their Activity as Oxygen Evolution Reaction Catalysts in Acidic Media, *Angew. Chem., Int. Ed.*, 2019, **58**, 4571–4575.

120 H. Chen, L. Shi, K. Sun, K. Zhang, Q. Liu, J. Ge, X. Liang, B. Tian, Y. Huang, Z. Shi, Z. Wang, W. Zhang, M. Liu and X. Zou, Protonated Iridate Nanosheets with a Highly Active and Stable Layered Perovskite Framework for Acidic Oxygen Evolution, *ACS Catal.*, 2022, **12**, 8658–8666.

121 X. Miao, L. Zhang, L. Wu, Z. Hu, L. Shi and S. Zhou, Quadruple perovskite ruthenate as a highly efficient catalyst for acidic water oxidation, *Nat. Commun.*, 2019, **10**, 3809.

122 Y. Lin, Z. Tian, L. Zhang, J. Ma, Z. Jiang, B. J. Deibert, R. Ge and L. Chen, Chromium-ruthenium oxide solid solution electrocatalyst for highly efficient oxygen evolution reaction in acidic media, *Nat. Commun.*, 2019, **10**, 162.

123 X. Liang, L. Shi, Y. Liu, H. Chen, R. Si, W. Yan, Q. Zhang, G.-D. Li, L. Yang and X. Zou, Activating Inert, Nonprecious Perovskites with Iridium Dopants for Efficient Oxygen Evolution Reaction under Acidic Conditions, *Angew. Chem., Int. Ed.*, 2019, **58**, 7631–7635.

124 A. L. Strickler, D. Higgins and T. F. Jaramillo, Crystalline Strontium Iridate Particle Catalysts for Enhanced Oxygen Evolution in Acid, *ACS Appl. Energy Mater.*, 2019, **2**, 5490–5498.

125 W. Liu, K. Kawano, M. Kamiko, Y. Kato, Y. Okazaki, I. Yamada and S. Yagi, Effects of A-site Cations in Quadruple Perovskite Ruthenates on Oxygen Evolution Catalysis in Acidic Aqueous Solutions, *Small*, 2022, **18**, 2202439.

126 M. A. Peña and J. L. G. Fierro, Chemical Structures and Performance of Perovskite Oxides, *Chem. Rev.*, 2001, **101**, 1981–2018.

127 P. P. Lopes, D. Y. Chung, X. Rui, H. Zheng, H. He, P. Farinazzo Bergamo Dias Martins, D. Strmcnik, V. R. Stamenkovic, P. Zapol, J. F. Mitchell, R. F. Klie and N. M. Markovic, Dynamically Stable Active Sites from Surface Evolution of Perovskite Materials during the Oxygen Evolution Reaction, *J. Am. Chem. Soc.*, 2021, **143**, 2741–2750.

128 C. Hu, J. Hong, J. Huang, W. Chen, C. U. Segre, K. Suenaga, W. Zhao, F. Huang and J. Wang, Surface decoration accelerates the hydrogen evolution kinetics of a perovskite oxide in alkaline solution, *Energy Environ. Sci.*, 2020, **13**, 4249–4257.

129 Z. Zhang, B. He, L. Chen, H. Wang, R. Wang, L. Zhao and Y. Gong, Boosting Overall Water Splitting via FeOOH Nanoflake-Decorated $PrBa_{0.5}Sr_{0.5}Co_2O_{5+\delta}$ Nanorods, *ACS Appl. Mater. Interfaces*, 2018, **10**, 38032–38041.

130 X. Liang, L. Shi, R. Cao, G. Wan, W. Yan, H. Chen, Y. Liu and X. Zou, Perovskite-Type Solid Solution Nano-Electrocatalysts Enable Simultaneously Enhanced Activity and Stability for Oxygen Evolution, *Adv. Mater.*, 2020, **32**, 2001430.

131 F. Yang, Y. Luo, Q. Yu, Z. Zhang, S. Zhang, Z. Liu, W. Ren, H.-M. Cheng, J. Li and B. Liu, A Durable and Efficient Electrocatalyst for Saline Water Splitting with Current Density Exceeding 2000 mA cm^{-2}, *Adv. Funct. Mater.*, 2021, **31**, 2010367.

132 L. A. King, M. A. Hubert, C. Capuano, J. Manco, N. Danilovic, E. Valle, T. R. Hellstern, K. Ayers and T. F. Jaramillo, A non-precious metal hydrogen catalyst in a commercial polymer electrolyte membrane electrolyser, *Nat. Nanotechnol.*, 2019, **14**, 1071–1074.

133 Q. Yang, G. Li, K. Manna, F. Fan, C. Felser and Y. Sun, Topological Engineering of Pt-Group-Metal-Based Chiral Crystals toward High-Efficiency Hydrogen Evolution Catalysts, *Adv. Mater.*, 2020, **32**, 1908518.

134 Y. Luo, Z. Zhang, M. Chhowalla and B. Liu, Recent Advances in Design of Electrocatalysts for High-Current-Density Water Splitting, *Adv. Mater.*, 2022, **34**, 2108133.

135 G. S. Ogumerem and E. N. Pistikopoulos, Parametric optimization and control for a smart Proton Exchange Membrane Water Electrolysis (PEMWE) system, *J. Power Sources*, 2020, **91**, 37–49.

136 P. Shirvanian and F. van Berkel, Novel components in Proton Exchange Membrane (PEM) Water Electrolyzers (PEMWE): Status, challenges and future needs. A mini review, *Electrochem. Commun.*, 2020, **114**, 106704.

137 W. Xiang, S. Liu and W. Tress, Interfaces and Interfacial Layers in Inorganic Perovskite Solar Cells, *Angew. Chem., Int. Ed.*, 2021, **60**, 26440–26453.

138 H. Zhang, W. Xiang, X. Zuo, X. Gu, S. Zhang, Y. Du, Z. Wang, Y. Liu, H. Wu, P. Wang, Q. Cui, H. Su, Q. Tian and S. Liu, Fluorine-Containing Passivation Layer via Surface Chelation for Inorganic Perovskite Solar Cells, *Angew. Chem., Int. Ed.*, 2023, **62**, e202216634.

139 L. Zhang, B. Li, J. Yuan, M. Wang, T. Shen, F. Huang, W. Wen, G. Cao and J. Tian, High-Voltage-Efficiency Inorganic Perovskite Solar Cells in a Wide Solution-Processing Window, *J. Phys. Chem. Lett.*, 2018, **9**, 3646–3653.